# NASA TECHNICAL NOTE

NASA TN D-5587

$e.1$

STATISTICAL DESIGN AND ANALYSIS
OF OPTIMUM SEEKING EXPERIMENTS TO
DEVELOP A GAMMA-PRIME STRENGTHENED
COBALT-NICKEL BASE ALLOY

by Gary D. Sandrock and Arthur G. Holms

Lewis Research Center
Cleveland, Ohio

NATIONAL AERONAUTICS AND SPACE ADMINISTRATION • WASHINGTON, D. C. • DECEMBER 1969

| 1. Report No. NASA TN D-5587 | 2. Government Accession No. | 3. Recipient's |
|---|---|---|

| 4. Title and Subtitle STATISTICAL DESIGN AND ANALYSIS OF OPTIMUM SEEKING EXPERIMENTS TO DEVELOP A GAMMA-PRIME STRENGTHENED COBALT-NICKEL BASE ALLOY | | 5. Report Date December 1969 |
|---|---|---|
| | | 6. Performing Organization Code |

| 7. Author(s) Gary D. Sandrock and Arthur G. Holms | 8. Performing Organization Report No. E-5023 |
|---|---|

| 9. Performing Organization Name and Address Lewis Research Center National Aeronautics and Space Administration Cleveland, Ohio 44135 | 10. Work Unit No. 129-03 |
|---|---|
| | 11. Contract or Grant No. |

| 12. Sponsoring Agency Name and Address National Aeronautics and Space Administration Washington, D.C. 20546 | 13. Type of Report and Period Covered Technical Note |
|---|---|
| | 14. Sponsoring Agency Code |

15. Supplementary Notes

16. Abstract

A previously developed NASA Co-base alloy was modified to achieve gamma-prime strengthening by the addition of Ni and Al. The levels of four of the eight elements in the composition were then optimized by the statistically founded Box-Wilson strategy of experimentation. The final as-cast alloy was characterized with regard to mechanical properties, oxidation resistance, and microstructure. The alloy is believed to have potential for aerospace applications.

| 17. Key Words (Suggested by Author(s)) Cobalt alloy  Statistical design Nickel alloy   of experiments Superalloys   Optimum seeking Gamma-prime strengthening Response surface methodology | 18. Distribution Statement Unclassified - unlimited |
|---|---|

| 19. Security Classif. (of this report) Unclassified | 20. Security Classif. (of this page) Unclassified | 21. No. of Pages 77 | 22. Price* $3.00 |
|---|---|---|---|

*For sale by the Clearinghouse for Federal Scientific and Technical Information
Springfield, Virginia 22151

# STATISTICAL DESIGN AND ANALYSIS OF OPTIMUM SEEKING EXPERIMENTS

## TO DEVELOP A GAMMA-PRIME STRENGTHENED

## COBALT-NICKEL BASE ALLOY

by Gary D. Sandrock and Arthur G. Holms

Lewis Research Center

## SUMMARY

A previously developed NASA cobalt-base alloy (Co-25W-1Ti-0.5Zr-3.12Cr-0.6C) was modified to achieve gamma-prime ($Ni_3Al$) strengthening by the addition of nickel and aluminum. The statistically founded Box-Wilson strategy of experimentation was then used to optimize the levels of titanium, chromium, carbon, and aluminum with respect to stress-rupture life. A factorial experiment was performed, followed by a vector of steepest ascent, in turn followed by another factorial experiment. This indicated the general region of a maximum. The acquisition of further data (star points and center points) allowed stress-rupture life to be expressed as a second-order polynomial function of composition. Canonical reduction of this equation indicated a family of compositions along a ridge of approximately constant stress-rupture life. The composition (charge) chosen for further evaluation was 37.4 cobalt - 38.0 nickel - 14.0 tungsten - 6.72 aluminum - 2.11 chromium - 1.01 titanium - 0.25 zirconium - 0.54 carbon. This alloy was designated NASA-SP.

NASA-SP was characterized as to several properties important to jet engine and other high-temperature aerospace applications. Its strength (stress-rupture and tensile) is equal to or superior to most cast cobalt-base alloys but inferior to the best nickel-base alloys. The alloy had somewhat lower intermediate-temperature ductility than is desirable, but had good high-temperature ductility. Oxidation tests showed the alloy to be comparable in oxidation resistance to the high chromium content, commercial cobalt-base alloys but again generally inferior to nickel-base alloys. Thermal fatigue resistance was also intermediate between nickel- and cobalt-base alloys. Phases observed in as-cast NASA-SP were gamma prime, titanium carbide, another carbide believed to be zirconium carbide, and an unidentified intermetallic phase rich in aluminum. Exposure to stress-rupture conditions coarsened the gamma prime and caused decomposition of the unknown intermetallic to gamma prime.

# INTRODUCTION

The program described herein had two main objectives:

(1) To achieve gamma-prime ($Ni_3Al$) strengthening of a previously developed NASA cobalt (Co)-base alloy by additions of aluminum (Al) and nickel (Ni)

(2) To use the statistically founded Box-Wilson strategy of experimentation in optimizing the composition

Although most Ni-base superalloys rely heavily on gamma-prime strengthening, its use has been very limited in Co-base alloys. Traditionally, Co-base alloys have used solid solution and carbide strengthening. However, a few examples of strengthening in Co-base alloys by gamma-prime or similar precipitates can be found. As early as 1956, the Co-base alloy J-1570 made use of $Ni_3Ti$ precipitation (ref. 1). More recently, work in Belgium (ref. 2) and Germany (ref. 3) has shown gamma-prime strengthening in several experimental Co-base alloys.

Statistically founded designs of experiments are not new in the area of optimization. They have been widely used in experimental work, but only to a limited extent in the field of alloy development. It is interesting that the previously mentioned $Ni_3Ti$ strengthened Co-base alloy J-1570 was developed more than a decade ago using a fractional-factorial experiment (ref. 1). More recently, the Ni-base superalloy NASA-TRW-VI-A was developed by fractional factorial and Latin square designs (ref. 4). The use of some elements of the Box-Wilson strategy (namely, the composite consisting of a factorial experiment and star design) in the development of a high strength stainless steel is described in reference 5.

The alloy used as a starting point in this investigation is based on the composition cobalt - 25 tungsten - 1 titanium - 1 zirconium - 3 chromium - 0.4 carbon (Co-25W-1Ti-1Zr-3Cr-0.4C) developed by Freche et al. at NASA Lewis (ref. 6). The alloy listed above was developed using argon melting techniques (ref. 6). Later, the use of vacuum melting, along with a more thorough determination of the optimum carbon content, led to a change from the composition reported in reference 6 to the following charge composition: Co-25W-1Ti-0.5Zr-3.12Cr-0.6C. (Unless otherwise noted, the charge composition in weight percent will be used to describe alloys in the remainder of this report.) This, then, represented the starting alloy in this investigation. Nickel and aluminum were added to this base alloy to achieve gamma-prime strengthening.

Once a gamma-prime strengthened alloy system had been established, the composition was empirically optimized. Several techniques for the experimental attainment of an optimum were available including random, single factor (one-at-a-time), and other strategies of experimentation. We used the statistically founded Box-Wilson strategy of optimum seeking (ref. 7) because of its potential superiority over the other techniques (ref. 8).

The Box-Wilson strategy led to a composition that we considered to be essentially

optimum with respect to stress-rupture life at the screening condition. This composition was then more completely characterized as to its physical metallurgy and various properties important to gas turbine and other high-temperature aerospace applications, such as strength and cyclic oxidation resistance.

# SYMBOLS

This list of symbols applies to all sections of the report except appendix F. The symbols of appendix F are defined therein.

$A$     matrix of coefficients of homogeneous quadratic form of regression equation

$a_o$     lattice parameter

$b$     estimate of $\beta$ from experiment

$F_i$     cumulative distribution function, eq. (B1)

$g$     number of independent variables (factors)

$i$     order number of coefficient, eq. (B1)

$n$     number of coefficients, eq. (B1)

$M$     modal matrix

$r$     length of vector, eq. (C2)

$s_j$     scale factor, eq. (A1)

$T$     temperature, $^oF$ ($^oC$)

$t$     time to failure (stress-rupture)

$U$     vector of $u_j$

$u_j$     translated coordinate axis

$V$     vector of coordinates of canonical form of regression equation

$\vec{V}$     vector of steepest ascent

$v_k$     translated and rotated coordinate axis

$X$     vector of coordinates of regression equation in design units

$x_j$     level of independent variable in design units

$Y$     random response variable

$y$     observed value of $Y$

$\beta$     unknown coefficient of a polynomial

$\epsilon$     random error

$\theta$     angle between $r$ and $x_1$ axis, eq. (C3)

3

$\lambda_k$     coefficients of canonically reduced equation

$\xi_j$     level of independent variables in natural units (wt. % or $^O$F ($^O$C))

$\sigma$     standard deviation

# BOX-WILSON STRATEGY OF OPTIMUM SEEKING

At this point, we shall give a general summary of the total Box-Wilson strategy. Certain mathematical points will be considered in greater detail in the appendixes. Other descriptions of the Box-Wilson strategy are Box and Wilson's original paper (ref. 7), an extensive review article (ref. 9), or the book by Davies (ref. 10).

The Box-Wilson strategy is compared with the more traditional single-factor or one-at-a-time strategy of attaining optimum conditions in figure 1. We have an unknown re-
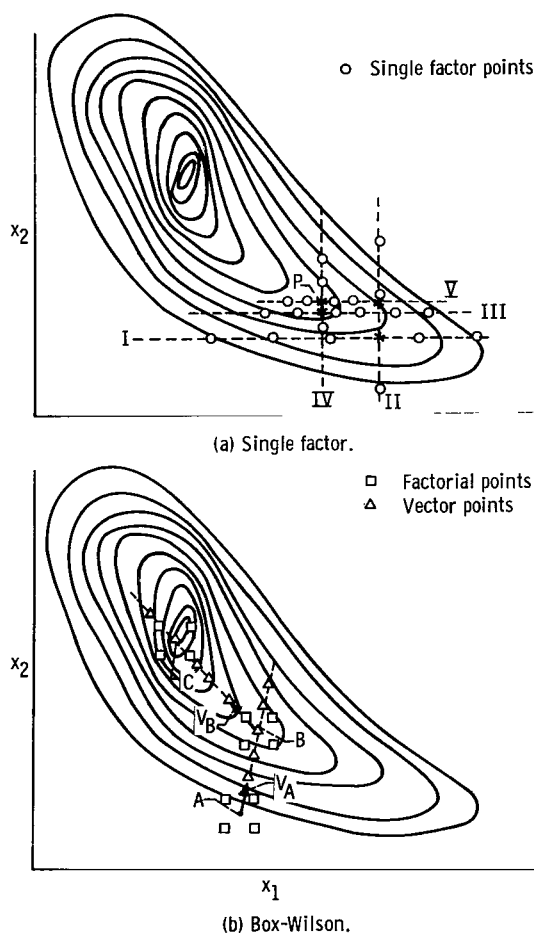


(a) Single factor.

(b) Box-Wilson.

Figure 1. - Strategies for experimental attainment of optimum conditions.

sponse surface (function of the independent variables) represented by the contour lines in the figure. These lines may represent lines of constant stress-rupture life, for example. We wish to optimize the response by adjusting the variables $x_1$ and $x_2$ which may be considered to be levels of two alloying elements.

First, consider the single factor method (fig. 1(a)). Normally, one variable $x_2$ is held constant, and the other $x_1$ is varied (as shown by line I in fig. 1(a)). After determining a maximum (shown by the asterisk), $x_1$ is held constant and $x_2$ is varied along line II until another maximum is found. Then $x_1$ is again varied but along line III, followed by another variation of $x_2$ along line IV, arriving at a maximum point P. Again $x_1$ is varied, this time along line V. On any of lines I, III, or V the response is so flat that the usual random error might completely mask the existence of a maximum along these lines. We might then incorrectly conclude that some point in this region, such as P, is the maximum.

The Box-Wilson strategy (fig. 1(b)) is loosely analogous to a blind man climbing a hill with the aid of a cane only. He feels the ground around himself to determine up, walks several paces in that direction and then again feels the ground around himself and again climbs a few paces in the direction of up. Repeating this over and over he will ultimately find himself at the summit where he can no longer find any up direction.

The Box-Wilson strategy can be separated into two distinct stages:

(1) the method of steepest ascent, which locates the general region of an optimum

(2) the method of local exploration, which more precisely locates the true optimum.

Consider first the method of steepest ascent. We usually have some knowledge or intuition as to where we might begin experimentation. Let this be point A in figure 1(b). As a first step, we would usually set up a factorial experiment about point A and make tests at two or more levels of $x_1$ and $x_2$. If we choose a two-level factorial experiment and wish to optimize the response with respect to not only two but say g variables $(x_1, x_2, x_3, \ldots, x_g)$, then the number of combinations of $x_1, x_2, x_3, \ldots, x_g$ for a full-factorial experiment would be $2^g$. However, this may lead to an impractically large number of tests so that fractional-factorial experiments are often substituted, whereby only some faction of the $2^g$ possible combinations are tested. Special two-level, full- and fractional-factorial designs intended for alloy development are given in reference 11. In the case of the two-level, two-variable experiment we show in figure 1(b) there are $2^2 = 4$ points for a full-factorial design. These are shown located in a rectangular array about the design center A.

The result of a factorial experiment is a set of estimated coefficients of a regression equation. If we limit the model (regression equation) to the second-order, it will have the form

$$Y = \beta_0 + \beta_1 x_1 + \beta_2 x_2 + \ldots + \beta_g x_g$$

$$+ \beta_{11} x_1^2 + \beta_{22} x_2^2 + \ldots + \beta_{gg} x_g^2$$

$$+ \beta_{12} x_1 x_2 + \beta_{13} x_1 x_3 + \ldots + \beta_{1g} x_1 x_g$$

$$+ \beta_{23} x_2 x_3 + \ldots + \beta_{2g} x_2 x_g$$

$$+ \ldots$$

$$+ \beta_{g-1, g} x_{g-1} x_g + \epsilon \qquad (1)$$

where $Y$ is the response (e.g., stress-rupture life), the $\beta$'s are the coefficients to be estimated from experimentation, and $\epsilon$ is a random error for which the average over a large number of observations is assumed to be zero. There are three types of coefficients in equation (1). Main effects $\beta_j$ involve only a single variable to the first order (e.g., $\beta_1 x_1$). Interaction effects $\beta_{jk}$ involve the product of two variables (e.g., $\beta_{12} x_1 x_2$). Finally, square terms $\beta_{jj}$ involve a single variable to the second order (e.g., $\beta_{11} x_1^2$). A factorial experiment estimates only main effects $\beta_j$ and interaction effects such as $\beta_{jk}$. As will be discussed later, the square terms $\beta_{jj}$ must be determined by an enlarged experiment.

For the purpose of steepest ascent, we assume that we are far enough away from the maximum so that the response surface is not very curved and we need use only first-order terms as follows:

$$Y = \beta_0 + \beta_1 x_1 + \beta_2 x_2 + \ldots + \beta_g x_g + \epsilon \qquad (2)$$

If the response surface is substantially curved, requiring interaction and/or square terms to describe it, the first-order model (eq. (2)) is not adequate and the method of steepest ascent should not be used. Rather we should go directly to the method of local exploration (to be described later).

Assume for the moment that the first-order model (eq. (2)) is valid. In the case of figure 1, $g = 2$. As will be developed, the constants $\beta_1$ and $\beta_2$, in essence, are the direction numbers of a vector $\vec{V}_A$ which points in the direction of the most rapid increase in the response $Y$ with respect to $x_1$ and $x_2$. In other words $\vec{V}_A$ points in the direction of the steepest ascent of the response hill from the design center A.

The second step is to run a series of tests along the direction of $\vec{V}_A$, shown by the

6

line of circular symbols in figure 1(b). At point B we would discover a maximum in the response along the vector. About this point we then set up a second factorial experiment and determine a second vector of steepest ascent $\vec{V}_B$. As before, we perform a number of tests in the direction of $\vec{V}_B$ until another maximum is reached (point C). On performing a third factorial experiment about C we would find no clearly defined direction of steepest ascent. From this we then conclude that we are in the vicinity of some kind of a stationary point, either a true summit or just a saddle point. At this point our simple first-order model (eq. (2)) is no longer able to describe the response surface, and we go to the method of local exploration.

Before beginning the discussion of local exploration, however, we shall make a few overall comments on the method of steepest ascent. Now, figure 1(b) is a fairly simple example where only two variables were considered. When there are more than two variables, we can no longer visualize the response surface in three-dimensional space but must go to a multidimensional space or hyperspace which we cannot graphically represent. Furthermore, depending on the complexity of the response surface and where the starting point just happens to be, it can often require more than the few factorial experiments we showed in our simple example to reach the vicinity of the maximum.

Once the general vicinity of the optimum has been located by the method of steepest ascent, our object is to locate the true optimum as precisely as possible by the method of local exploration. That method is somewhat more involved experimentally and mathematically. Only a brief outline will be given here. More detail will be presented during the discussion of the actual results of this investigation.

The first step is to determine a new model (equation) which will adequately describe the response surface in the vicinity of the maximum found along the vector of steepest ascent. As mentioned earlier, the first-order (linear) equation (eq. (2)) used in the method of steepest ascent is not adequate. This is because substantial curvature of the response surface exists around the summit or optimum. Often a second-order equation of the form of equation (1) will suffice. To determine the coefficients of the squared terms (i.e., $\beta_{jj}$) several more tests in addition to those of a factorial experiment are necessary. The coordinates of these tests are called star points and will be discussed in the results section.

After determining the coefficients $\beta_j$, $\beta_{jj}$, and $\beta_{jk}$, equation (1) is then differentiated with respect to all variables to determine the point of zero slope or stationary point. This stationary point may represent a true maximum or just a saddle point (also known as a col or minimax). A mathematical procedure called the method of canonical reduction (ref. 10) is used to determine which one the stationary point actually represents. If a saddle point is indicated, then further experimentation along a rising ridge can lead to improved response. If a true maximum is indicated, then the stationary point may be considered the optimum, and the procedure is finished. The whole procedure is summarized in the form of a flow chart by figure 2.
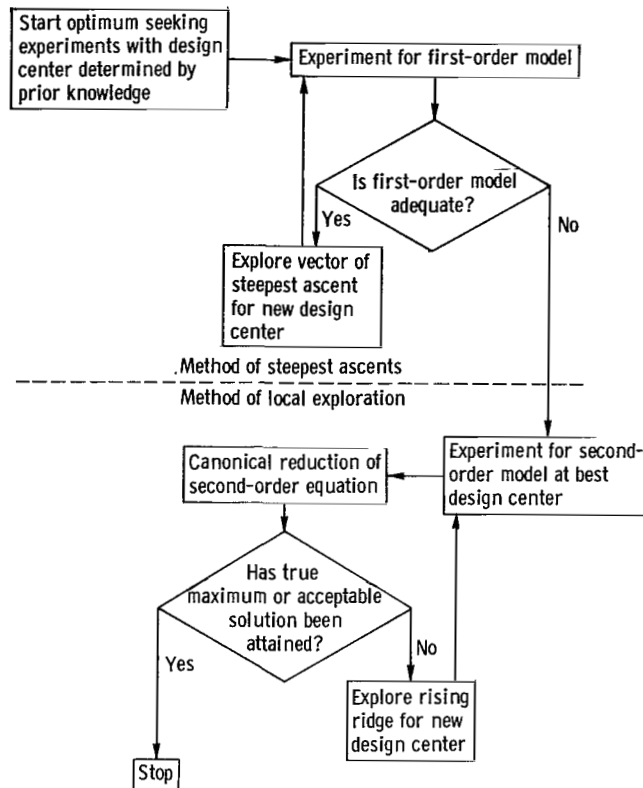
Figure 2. - Box-Wilson methods.

The Box-Wilson strategy can have several advantages over the single-factor strategy, depending on the complexity of the response surface one is dealing with:

(1) It may prevent one from overlooking an optimum as illustrated in the discussion of figure 1(a); that is, there is a greater confidence in the results.

(2) It allows the determination of interactions between variables that can only indirectly be observed in the single-factor method. In other words, the best combination of several variables is more efficiently determined.

(3) It can, under most circumstances, result in more efficient experimentation. The somewhat greater efficiency of the Box-Wilson strategy over other empirical optimum seeking procedures is indicated in reference 8.

## EXPERIMENTAL PROCEDURE

### Specimen Preparation

With the exception of a few preliminary arc-melted buttons, all specimens were pre-

TABLE I. - RAW MATERIALS

| Element | Form | Quoted purity |
|---------|------|---------------|
| Co | Electrolytic | 99.9+ (Co + Ni) |
| Ni | Electrolytic | 99.9+ |
| W | Powder | 99.9+ |
| Al | Pellets | 99.8+ |
| Cr | Electrolytic | 99.8+ |
| Ti | Sponge | 99.3+ |
| Zr | Sponge | 99.9+ |
| C | Granular graphite | 98+ |

pared by vacuum induction melting of virgin material. The forms and purities of the raw materials are given in table I.

The preliminary metallographic button specimens were made with a small button melting arc-furnace. Approximately 50-gram specimens were prepared using a nonconsumable tungsten electrode, a water-cooled copper hearth, and approximately 300-ampere direct current. Melting was done in argon at about 200 torr ($2.7 \times 10^4$ N/m$^2$) pressure. The buttons were turned and remelted four or five times to insure thorough mixing. In the button melts Ni and Al were melted in the atomic proportions of 3 Ni to 1 Al, along with a pellet of the previously induction melted base alloy (Co-25W-1Ti-0.5Zr-3.12Cr-0.6C).

Induction melting was done in stabilized zirconia (ZrO$_2$) crucibles. Charge weights were 1.6 kg. The melting sequence was as follows:

(1) A cold charge of Co, Ni, W, and C was placed in a new ZrO$_2$ crucible. Pumping was started and continued until a standard "leak-up" rate was achieved (more than 0.4 min for a pressure rise of $10^{-2}$ torr (1.3 N/m$^2$)). Then power was applied to the crucible.

(2) At the first signs of melting the chamber was back-filled to 40 torr (5.3 kN/m$^2$) of argon to prevent excessive splashing during the initial melt-down.
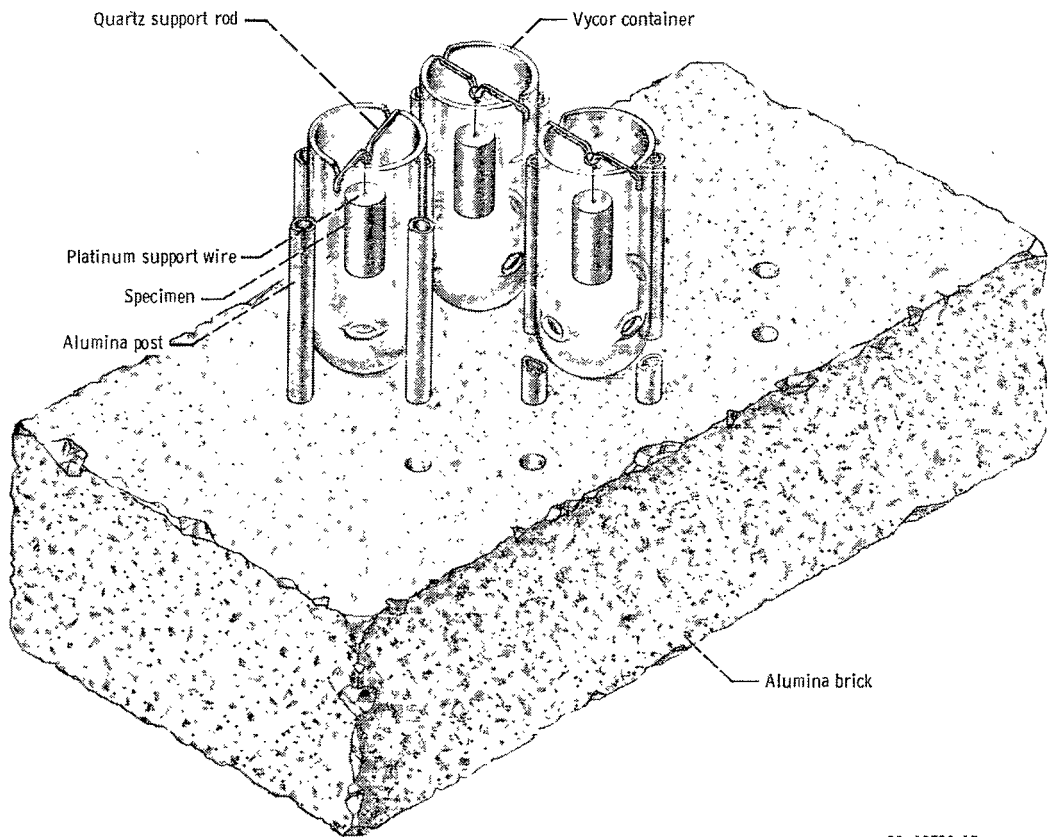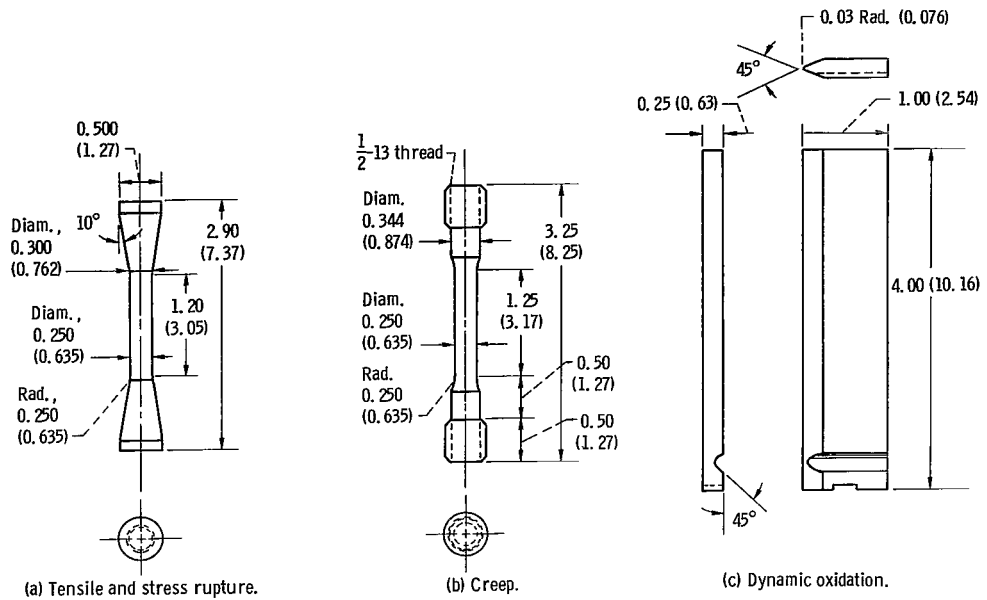
(3) After all Co, Ni, W, and C were melted, the chamber was evacuated and a gentle carbon-boil maintained for 20 minutes. Pressure during this period was generally below $10^{-2}$ torr (1.3 N/m$^2$).

(4) Chromium was then added under an argon pressure of 40 torr (5.3 kN/m$^2$).

(5) The chamber was again evacuated, and Al, Ti, and Zr were added.

(6) The charge was next heated to about 3075° F (1690° C) and then cooled to the desired pouring temperature. The temperature-time profile after step (5) was carefully duplicated from casting to casting so that the Al evaporation was the same each time.

(7) Shortly before the melt had cooled to the pour temperature, the chamber was backfilled to 15 torr (2.0 kN/m$^2$) of argon. Finally, the melt was poured when the desired temperature had been reached. During the melting sequence, the melt temperature

(a) Tensile and stress rupture.

0.500
(1.27)

Diam.,
0.300
(0.762)

10°

2.90
(7.37)

Diam.,
0.250
(0.635)

1.20
(3.05)

Rad.,
0.250
(0.635)

(b) Creep.

½-13 thread

Diam.
0.344
(0.874)

3.25
(8.25)

Diam.
0.250
(0.635)

1.25
(3.17)

Rad.
0.250
(0.635)

0.50
(1.27)

0.50
(1.27)

(c) Dynamic oxidation.

0.03 Rad. (0.076)

45°

0.25 (0.63)

1.00 (2.54)

4.00 (10.16)

45°

Quartz support rod

Vycor container

Platinum support wire

Specimen

Alumina post

Alumina brick

CD-10508-17

(d) Static oxidation specimens shown in test fixture. Specimen dimensions: 0.225 (0.57 cm) inch diameter; 0.5 (1.27 cm) inch long.

Figure 3. – Specimens used (Dimensions are in inches (cm)).

10

was measured by means of an optical pyrometer corrected for sight glass absorption.

The mold was a zircon shell which was imbedded in fire-clay grog and held at 1600° F (871° C) by a resistance mold heater. Each casting consisted of a cluster of test bars of one of the shapes shown in figure 3. Stress-rupture specimens (fig. 3(a)) and dynamic oxidation specimens (fig. 3(c)) were cast to size. The threaded creep specimens (fig. 3(b)) were cast somewhat oversized and machined to the dimensions shown. Static oxidation specimens (fig. 3(d)) were machined from cast stress-rupture bars (fig. 3(a)). After casting, the molds were allowed to remain in the vacuum chamber for 15 minutes. They were then removed and allowed to cool to room temperature (about 6 hr) before knockout and cutoff. Before testing, all specimens were vapor blasted and inspected by radiographic and fluorescent penetrant techniques. Chemical analyses of selected heats were made by wet chemical methods for each set of melts.

## Mechanical Testing

Stress-rupture tests were run on constant-load 10 to 1 or 20 to 1 lever arm machines using resistance wound furnaces. All tests were run in air. Specimens run at 1500° and 1700° F (816° and 927° C) were instrumented with Chromel-Alumel thermocouples, and those run at 1850° and 2000° F (1010° and 1093° C) with platinum 13-percent rhodium/platinum thermocouples. Specimens were heated to temperature and loaded in a period of 3 to 6 hours. Temperature control during the tests was maintained essentially within ASTM recommended limits.

A few creep tests were run. These were performed in a manner similar to the stress-rupture tests except that a slightly different specimen was used (see fig. 3(b)) that would allow the use of mechanical extensometers clamped to each shoulder. An elongation data point was electronically recorded once every minute from the output of a calibrated differential transformer. The fillet to fillet distance was used as the effective gage length.

Tensile tests were also run in air using a resistance furnace. Heating time was about 1 hour. The tensile machine was hydraulically operated and did not have a precise strain-rate control. However, by using a constant valve setting, an approximately constant strain rate was achieved (estimated at 3 to 6 percent per min after yield).

## Oxidation Tests

Cyclic oxidation tests were run with the optimized alloy both in still air and a high-velocity gas stream. Specimens run in static air were cylinders 0.225 inch in diameter and 0.5 inch long (0.57 and 1.27 cm). They were machined from the test section of cast

stress-rupture bars and finished with 600-grit silicon carbide paper. As shown in figure 3(d), they were suspended in open Vycor crucibles by platinum wires spot welded to one end. The crucibles, in turn, were placed on an alumina brick. The entire assembly was then placed in a furnace preheated to $1800^{\circ}$ F ($982^{\circ}$ C). After an oxidation time of 100 hours in static air, the entire assembly was removed and air cooled to room temperature. The specimens cooled in approximately 15 minutes. Weight gain and amount to spall were determined. The cycle was then repeated three more times for a total of 400 hours at temperature.

The details of the equipment used in the high-velocity oxidation tests are given in reference 12. Briefly, a paddle-wheel of specimens of the configuration shown in figure 3(c) was rotated in the combustion products of a natural gas burner. Gas velocity was approximately Mach 1 at the nozzle exit and specimen temperature was maintained at $2000^{\circ}$ F ($1093^{\circ}$ C). A cycle consisted of 1 hour at temperature followed by cooling for 3 minutes in a blast of room temperature air. Specimens reached room temperature in 1.5 minutes. One-hundred cycles were run. Specimens were inspected every 20 cycles for weight change and thermal fatigue cracking.

## Metallography and Analytical Techniques

Metallographic specimens were prepared by mechanical polishing through 0.05-micrometer alumina. Specimens for optical microscopy were etched by immersion in a solution of 33 parts water, 33 parts glacial acetic acid, 33 parts concentrated nitric acid, and 1 part concentrated hydrofluoric acid. Specimens for replica electron microscopy were etched lightly in Murakami's reagent (10 g potassium ferricyanide, 10 g potassium hydroxide, and 100 ml water). Macroetching was done in concentrated hydrochloric acid with about 5 percent hydrogen peroxide.

Samples for phase identification were residues obtained by electrolytic separation (extraction) in an aqueous solution of 1 weight percent each of ammonium sulfate and citric acid used by Kriege and Sullivan for the Ni-base alloy Udimet 700 (ref. 13). The procedure was essentially the same as that of reference 13, except that a much lower current density of approximately 0.005 ampere per square centimeter was necessary to avoid total dissolution of the gamma-prime.

X-ray diffraction patterns of extracted residues and oxide samples were made using a standard 114.6-millimeter Debye-Scherrer camera. Either Ni filtered copper or vanadium filtered Cr radiation was used.

One cast specimen of the optimized alloy was studied using an electron microprobe analyzer. Back-scattered-electron and X-ray image photographs (area scans) were made at a magnification of 500 with Co, Ni, W, Al, Cr, Ti, Zr, and C radiations. Microprobe

conditions were 17 kilovolts and 0.3 microampere. These photographs give a representation of the distribution of the alloying elements in the microstructure.

## RESULTS AND DISCUSSION

## Preliminary Survey

As explained in the INTRODUCTION, the starting point or base alloy was the previously developed Co-25W-1Ti-0.5Zr-3.12Cr-0.6C (charge composition). The first step in the program was to determine whether a stable gamma-prime precipitate could be introduced into the alloy, and if so, to determine whether worthwhile strength properties were likely.

To determine whether gamma-prime could be stabilized at high temperature in the alloy, a series of metallographic specimens were prepared by arc melting small buttons. Pieces of the base alloy were melted along with 0, 15, 30, and 45 weight percent Ni + Al in the atomic ratio of 3Ni to 1Al. In other words, the base alloy was effectively diluted with various amounts of $Ni_3Al$. The specimens were aged at $1850^\circ$ F ($1010^\circ$ C) and examined metallographically for the presence of precipitates. The resultant microstructures for the base alloy and the 45 percent Ni + Al alloy are shown in figure 4. The base alloy button melt (fig. 4(a)) showed the coarse interdendritic carbide network seen before in investment castings of this alloy series (ref. 6). Only a small amount of fine precipitate, which was especially noticeable near the carbide network, had developed. However, the alloy with 45 percent Ni + Al (fig. 4(b)) showed a profusion of cubically shaped precipitate particles typical of the gamma-prime seen in Ni-base superalloys (ref. 14). The 15 and 30 percent Ni + Al specimens (not shown) showed a much lesser amount of gamma-prime. Thus we had microstructural evidence that a substantial amount of gamma-prime could be introduced into the base alloy by addition of 45-weight-percent Ni + Al. The composition of this alloy, of course, looks quite different from the original base because of the heavy dilution. The composition of the base + 45 percent Ni + Al is approximately 39Co-38Ni-14W-0.5Ti-0.25Zr-1.75Cr-0.35C-6Al (in wt. %).

Having metallographic indication that substantial amounts of gamma-prime were present, we next determined whether the high-temperature strength of the modified alloy was sufficiently high to warrant further study. For that purpose, test bars (fig. 3(a)) of the new alloy were made by the induction melting procedure described earlier using a pour temperature of $3050^\circ$ F ($1677^\circ$ C). Metallography of as-cast specimens indicated a fine optically irresolvable precipitate, presumed to be gamma-prime formed during cooling of the casting. Stress-rupture tests at $1850^\circ$ F ($1010^\circ$ C) and 15 ksi ($103$ MN/m$^2$) of as-cast bars resulted in an average life of about 75 hours. This com-
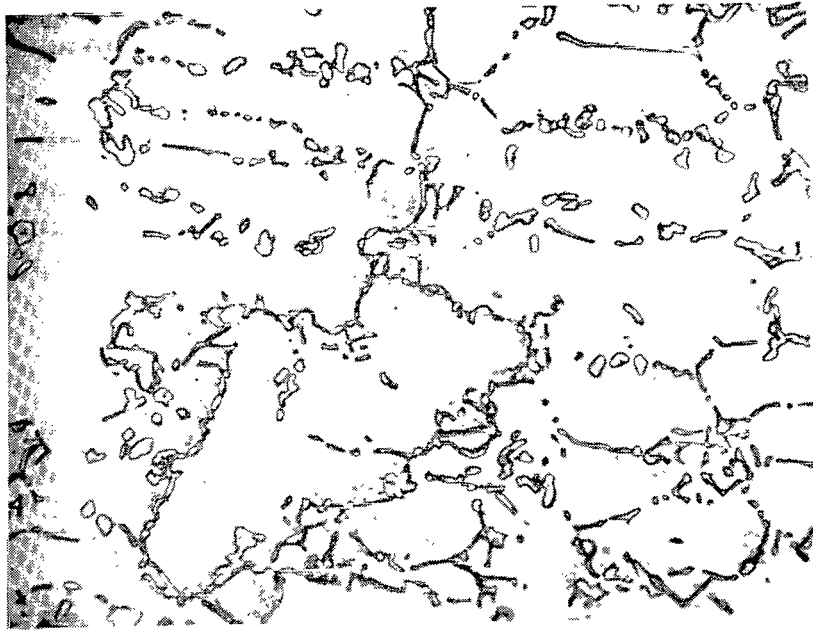
(a) Base alloy (Co-25W-1Ti-0.5Zr-3.12Cr-0.6C).
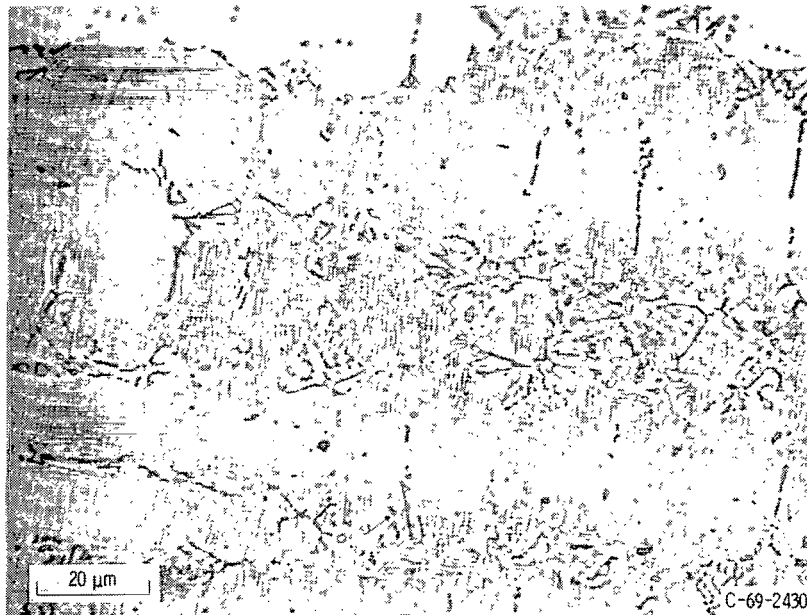


(b) Base alloy plus 45 weight percent Ni₃Al.

Figure 4. – Effect of adding nickel and aluminum to base alloy. Microstructures after ageing 150 hours at 1850° F (1010° C). X750.

pares with approximately 100 hours for the starting alloy Co-25W-1Ti-0.5Zr-3.12Cr-0.6C.

Because of the possible participation of Co in forming a gamma-prime of the type (Ni, Co)$_3$Al, we felt that increases in Al above 3Ni to 1Al, might be helpful in increasing stress-rupture life. Therefore, a single-factor variation of Al was made. This is shown in figure 5. Increasing the Al addition from 6 to 7 percent increased the average life from 75 to about 200 hours. Increasing the levels of Al above 7 percent gave decreased life.
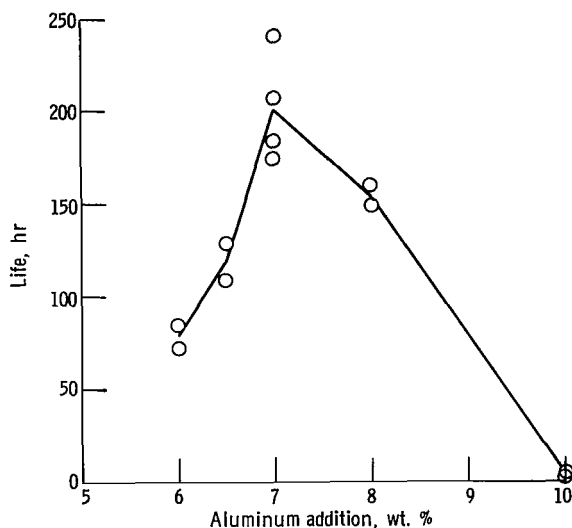


Figure 5. - Effect of aluminum addition on stress-rupture life of alloy Co-38Ni-14W-0.5Ti-0.25Zr-1.75Cr-0.35C. Temperature, 1850° F (1010° C); stress, 15 ksi (103 MN/m$^2$).

To summarize, preliminary studies showed a high-temperature strength potential for a high-cobalt, gamma-prime-strengthened alloy series of the following approximate composition: 38Co-38Ni-14W-0.5Ti-0.25Zr-1.75Cr-0.35C-7Al (designated GP-2). The next step was an attempt to optimize the response with respect to the levels of several elements simultaneously using the Box-Wilson strategy of experimentation.

## Optimization

Approach. - We had to ask ourselves two questions: The first was, what property shall we consider to be the response; that is, what property shall we optimize - stress-rupture life, high-temperature tensile strength, oxidation resistance, etc.? In order to

use the Box-Wilson method conveniently, we decided to consider only that property in which we were most interested, namely, stress-rupture life, and largely ignore the other properties. This may not always be the best approach to take, because in practice an application frequently requires an alloy that is a compromise among several properties.

Three techniques are available for optimization problems that require compromises among properties (dependent variables).

(1) The basis of the compromise might be expressed in quantitative terms defining a new single dependent variable (e. g. , a weighted average of several properties) that would be optimized.

(2) One of the dependent variables might be optimized under the constraint that the other dependent variables are to be held within certain limits.

(3) The response function for the most important dependent variable could be determined in the vicinity of its optimum. A canonical reduction could then be used to identify those combinations of the independent variables that would provide for the improvement of a second dependent variable, while maintaining the value of the first dependent variable essentially constant. This technique was adopted in the present investigation, in which the second dependent variable was the ductility (elongation).

For the primary dependent variable (stress-rupture life), we chose the single temperature and stress combination of $1850^o$ F and 15 ksi ($1010^o$ C and 103 MN/m$^2$). This was done to keep the number of tests to a minimum and again to create a single unambiguous dependent variable.

The second question we asked ourselves was with respect to which of the eight elements in the alloy do we wish to optimize the response? Again to minimize testing, we limited the variables to the four elements that we considered to be most important to the stress-rupture strength:

    (1) Titanium, because it takes an active role in the formation of both gamma-prime and MC carbides

    (2) Chromium, because it is generally considered to be detrimental to high-temperature strength yet important to good corrosion resistance

    (3) Carbon, because it is used in almost all superalloys to produce carbide strengthening

    (4) Aluminum, because it produces the strengthening gamma-prime precipitate

In all the compositions made in the optimization part of the program, these elements were varied at the expense of the cobalt content. Nickel, tungsten, and zirconium were held constant at 38, 14, and 0.25 weight percent, respectively.

First factorial experiment. - For the first experiment, pour temperature was included as a variable along with the four previously mentioned elements; this made a total of five variables. A two-level, full-factorial experiment would have required $2^5$ = 32 compositions. For the purpose of steepest ascent, however, the comprehensive information a full-factorial experiment gives on interactions is really not necessary. So

16

we used a half-replicate experiment requiring only 16 melts. The experiment design (i. e., the 16 combinations of high and low levels) was taken from table 7 of reference 11. It is common to describe the levels in design units away from the design center. The actual design center and levels we used are given in natural units (charge wt. %) in table II(a) along with the scale factors for converting to design units (see appendix A for details of this conversion). Using these scale factors, the levels in natural units were converted to design units for the 16 compositions and are listed in table II(b). In design units, then, +1 indicates the high level of the respective element and -1 the low level.

Metallurgical judgment is important in choosing the conditions for an initial experiment. Although theoretically the same optimum should be achieved in the end, a judicious choice of initial conditions can result in fewer factorial experiments and steepest ascents to reach the vicinity of the optimum.

The design center and absolute levels chosen (in natural units) were somewhat, but not completely arbitrary except for Al, which we had already surveyed by single-factor variation (fig. 5). This survey established a promising preliminary alloy: 38Co-38Ni-14W-0. 5Ti-0. 25Zr-1. 75Cr-0. 35C-7Al (GP-2). This was the best available alloy, according to prior experimentation, and as such would have been a reasonable design center composition for a starting point of the Box-Wilson procedure. However, it was not so used because certain prior metallurgical concepts suggested that higher levels of Ti and Cr were preferred. Titanium was increased in hopes of achieving more gamma-prime and carbide strengthening. Chromium was increased in hopes of achieving some improved oxidation resistance without loss in strength. Carbon was varied above and below the level of the preliminary alloy. Because of the indicated sharp peak in the Al curve (fig. 5), it was varied tightly around 7 percent. The design center, then, was 1. 0Ti, 4. 0Cr, 0. 4C, 7. 0Al, and $2900^\circ$ F ($1593^\circ$ C) pour temperature.

One casting was made for each of the 16 compositions in table II(b). Two stress-rupture tests from each composition were run at $1850^\circ$ F and 15 ksi ($1010^\circ$ C and 103 $MN/m^2$). The results are also shown in table II(b). Testing variability and variability within castings could be observed from the test bar duplicates, but there were no melt to melt duplicates and therefore melt-to-melt variability could not be observed. A later investigation of melt-to-melt variability showed that the melt-to-melt variability significantly exceeded the bar-to-bar variability.

As the next step, the estimated coefficients of a regression equation were determined from the data (table II(b)) using a simple arithmetic procedure called the Yates method (see ref. 10). Before doing this, however, the value of the response (stress-rupture life = t) was transformed to the form $y = \log t$, to generate a variable whose variance (scatter) would be approximately constant over large changes in stress-rupture life that might result from small changes in composition. A value of $\log t$ was determined for each test. The mean value of $\log t$ was computed for the two tests from each melt. These values of mean $\log t$ were then introduced into the Yates procedure and the coef-

## TABLE II. - FIRST FACTORIAL EXPERIMENT, ONE HALF

## REPLICATE OF $2^5$

### (a) Levels of independent variables in natural units

[Contents of Ni, W, and Zr held constant at 38, 14, and 0.25 wt. %, respectively; balance, Co.]

| Variable | Design center | Lower level | Upper level | Scale factor |
|----------|---------------|-------------|-------------|--------------|
| | Level, wt. % | | | |
| $\xi_{Ti}$ | 1.0 | 0.5 | 1.5 | 0.5 |
| $\xi_{Cr}$ | 4.0 | 2.0 | 6.0 | 2.0 |
| $\xi_C$ | .4 | .3 | .5 | .1 |
| $\xi_{Al}$ | 7.0 | 6.75 | 7.25 | .25 |
| $\xi_T$ $^o$F ($^o$C) | 2900 (1593) | 2850 (1566) | 2950 (1621) | 50 (28) |

### (b) Levels of independent variables in design units and corresponding results

| Alloy | Levels | | | | | Stress-rupture[a] life, hr | Elongation,[a] % |
|-------|--------|--------|-------|----------|-------|-----------|-------------|
| | $x_{Ti}$ | $x_{Cr}$ | $x_C$ | $x_{Al}$ | $x_T$ | | |
| 1 | -1 | -1 | -1 | -1 | -1 | 175.1, 199.4 | 31, 15 |
| 2 | +1 | -1 | -1 | -1 | +1 | 83.2, 166.5 | 4, 8 |
| 3 | -1 | +1 | -1 | -1 | +1 | 22.9, 24.5 | 9, 8 |
| 4 | +1 | +1 | -1 | -1 | -1 | 14.7, 21.1 | 3, 8 |
| 5 | -1 | -1 | +1 | -1 | +1 | 153.5, 237.6 | 13, 22 |
| 6 | +1 | -1 | +1 | -1 | -1 | 119.5, 129.6 | 10, 10 |
| 7 | -1 | +1 | +1 | -1 | -1 | 28.2, 39.0 | 17, 14 |
| 8 | +1 | +1 | +1 | -1 | +1 | 30.0, 38.1 | 14, 11 |
| 9 | -1 | -1 | -1 | +1 | +1 | 55.1, 79.2 | 11, 10 |
| 10 | +1 | -1 | -1 | +1 | -1 | 29.2, 47.0 | 5, 8 |
| 11 | -1 | +1 | -1 | +1 | -1 | 3.5, 11.1 | 10, 15 |
| 12 | +1 | +1 | -1 | +1 | +1 | 17.7, 19.6 | 14, 13 |
| 13 | -1 | -1 | +1 | +1 | -1 | 132.1, 190.7 | 19, 16 |
| 14 | +1 | -1 | +1 | +1 | +1 | 94.1, 95.1 | 10, 9 |
| 15 | -1 | +1 | +1 | +1 | +1 | 12.7, 19.1 | 21, 10 |
| 16 | +1 | +1 | +1 | +1 | -1 | 16.7, 16.8 | 18, 15 |

[a]At stress of 15 ksi (103 MN/m$^2$) and temperature of 1850$^o$ F (1010$^o$ C).

ficients of a regression equation were estimated. That equation, written in order of decreasing absolute values of the coefficients is

$$\log t = 1.652 - 0.383\, x_{Cr} - 0.146\, x_{Al} + 0.100\, x_C + 0.078\, x_{Ti}x_{Cr} + 0.052\, x_{Ti}x_T - 0.045\, x_C x_T + 0.042\, x_C x_{Al}$$

$$+ 0.037\, x_T + 0.036\, x_{Cr}x_T + 0.033\, x_{Ti}x_{Al} - 0.029\, x_{Ti} + 0.022\, x_{Al}x_T - 0.016\, x_{Ti}x_C - 0.003\, x_{Cr}x_C \qquad (3)$$

$$- 0.002\, x_{Cr}x_{Al}$$

the level of each variable being expressed in design units.

At this point significance tests were made to determine which effects were larger than random experimental error. Because of the lack of melt to melt duplication, conventional tests of significance could not be used. One approach that was used is "half-normal plotting," and the construction and interpretation of such plots is described in reference 15. Such a plot is shown by figure 6, in which the abscissa values are the ordered absolute values of the coefficients of equation (3). As discussed in appendix B, the coefficients that are indicated by figure 6 as being significant for this experiment are the one to four largest values, namely, the coefficients of Cr, Al, C, and TiCr in decreasing order of indicated significance.

The second approach used consisted of "chain pooling." That kind of analysis of the present experiment was given in the discussion of table V of reference 16, in which the coefficients of the Cr and Al terms of equation (3) were concluded to be clearly significant and the coefficients of the C and TiCr terms were concluded to be of possible significance. All other coefficients were concluded to be insignificant.

As far as the main effects are concerned, the increase of Cr and Al was harmful to stress-rupture life, and the increase of C beneficial to stress-rupture life. Titanium and
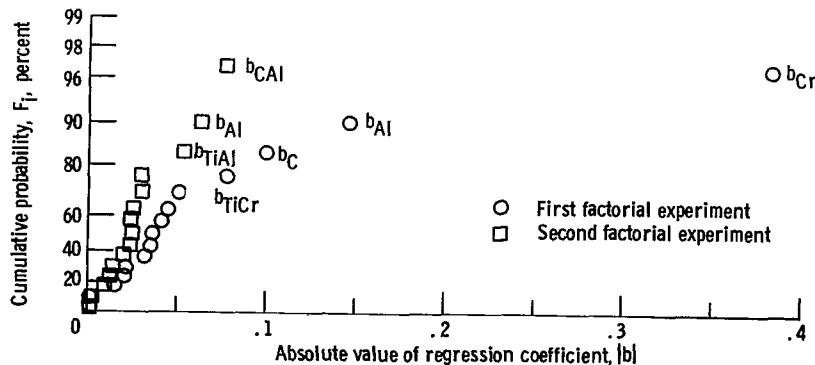


Figure 6. - Half-normal plots.

pour temperature were unimportant (except for the possible TiCr interaction effect). Of these four effects the two-factor interaction is the least significant; therefore, the assumption was made that the response surface is sufficiently planar so that the method of steepest ascents would be useful in determining a direction of improved response. The stage of experimenting is now equivalent to the branch point of figure 2 labeled "Is first-order model adequate?" The decision procedure has answered "Yes" and, as indicated in figure 2, the next step is to explore the vector of steepest ascent to obtain a new design center.

Steepest ascent. - Neglecting the interaction terms, we can rewrite equation (3) in terms of only main effects as follows:

$$\log t = 1.652 - 0.383\ x_{Cr} - 0.146\ x_{Al} + 0.100\ x_C + 0.037\ x_T - 0.029\ x_{Ti} \qquad (4)$$

The coefficients of the main effects may be considered to be the direction numbers of a vector in multidimensional space. Points along this vector represent the steepest ascent of the response "hill." The technique for computing a sequence of compositions along such a vector is given in the appendix C. The levels of each variable were changed as dictated by the signs and relative magnitudes of the main effects (eq. (4)). For the sake of completeness all main effects were considered, even the insignificant Ti and T. We made and tested four compositions along the vector as listed in table III. Point 1 represents the design center of the experiment. Points 2 and 3 are points along the vector, chosen by arbitrary decrements of Cr. Point 4 is really a pseudo-vector-point because Cr was held at zero (level of point 3) and the other variables changed as if a level of minus 2 percent Cr were present. It should be noted that the stated variations of pour temperature are somewhat artifical because they are too small to be experimentally distinguishable.

TABLE III. - STEEPEST ASCENT POINTS

[Contents of Ni, W, and Zr held constant at 38, 14, and 0.25 wt. %, respectively; balance, Co.]

| Point | Composition, wt. % | | | | Pour temperature, | | Stress-rupture life,[a] hr | Elongation,[a] % |
|-------|------|-----|-------|------|------|------|------|------|
| | Ti | Cr | C | Al | °F | °C | | |
| 1 | 1.00 | 4.0 | 0.400 | 7.00 | 2900 | 1593 | 60.3, 55.6 | 6, 8 |
| 2 | .96 | 2.0 | .426 | 6.90 | 2905 | 1596 | 101.6, 92.1 | 12, 10 |
| 3 | .92 | 0 | .452 | 6.81 | 2910 | 1599 | 141.9, 171.1 | 12, 13 |
| 4 | .88 | 0 | .478 | 6.71 | 2915 | 1602 | 116.0, 133.7 | 9, 14 |

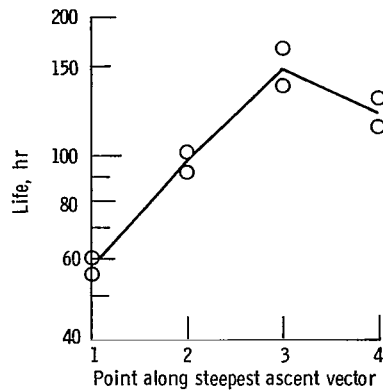[a]At stress of 15 ksi (103 MN/m$^2$) and temperature of 1850° F (1010° C).

Figure 7. - Stress-rupture life at 1850° F and 15 ksi (1010° C and 103 MN/m²) as function of position along steepest ascent vector. (See table III.)

The results given in table III are also plotted in figure 7. As expected, life increased in moving along the steepest ascent vector. Maximum life was obtained with point 3.

Second factorial experiment. - The results shown by table III and figure 7 suggest that further experimentation be carried on in the vicinity of point 3 (0.92 Ti, 0 Cr, 0.452 C, 6.81 Al, and 2910° F (1599° C) pour temperature). However, a new design center need not coincide exactly with point 3. Because the pour temperature had been found to be insignificant in the first factorial experiment and because the changes in pour temperature called for in the vector experiment were essentially negligible quantities, the decision was made to fix the pour temperature at the original design center (2900° F (or 1593° C)). Because Cr had only been investigated at widely spaced intervals (table III), we decided to retain it at a nonzero level. The indicated level of Al (vector point 3) was rounded from 6.81 percent to 6.75 percent . The indicated level of carbon was rounded from 0.452 to 0.5 percent. The first-factorial experiment had suggested that the first degree effect of Ti was not significant but that an interaction between Ti and Cr might be significant. The decision was therefore made to continue the investigation of Ti in the range thought to be important.

The new design center and the new levels chosen for the factorial design are shown in table IV(a). The Al and C were varied over ranges that are close to the previously exhibited optimum point (point 3 of table III and fig. 7). The Cr was varied about the somewhat arbitrary value of 2 percent. Because the role of the Ti had not been made clear, we varied it over wide ratios of its design center value as was done in the first factorial experiment.

For several reasons we decided to run a full-factorial experiment requiring $2^4 = 16$ melts rather than a fractional replicate. In order to determine the first-degree coefficients with small errors of estimate, 16 compositions should not be considered ex-

21

## TABLE IV. - SECOND FACTORIAL EXPERIMENT, FULL

## REPLICATE OF $2^4$

### (a) Levels of independent variables in natural units

[Contents of Ni, W, and Zr constant at 38, 14, and 0.25 wt. %, respectively; balance, Co.]

| Variable | Design center | Lower level | Upper level | Scale factor |
|---|---|---|---|---|
| | Level, wt. % | | | |
| $\xi_{Ti}$ | 1.0 | 0.5 | 1.5 | 0.5 |
| $\xi_{Cr}$ | 2.0 | 1.5 | 2.5 | .5 |
| $\xi_C$ | .5 | .4 | .6 | .1 |
| $\xi_{Al}$ | 6.75 | 6.5 | 7.0 | .25 |

### (b) Levels of independent variables in design units and corresponding results

| Alloy | Levels | | | | Stress-rupture[a] life, hr | Elongation,[a] % |
|---|---|---|---|---|---|---|
| | $x_{Ti}$ | $x_{Cr}$ | $x_C$ | $x_{Al}$ | | |
| 1 | -1 | -1 | -1 | -1 | 126.7, 176.5 | 13, 12 |
| 2 | +1 | -1 | -1 | -1 | 196.0, 184.1 | 10, 8 |
| 3 | -1 | +1 | -1 | -1 | 163.4, 152.6 | 24, 12 |
| 4 | +1 | +1 | -1 | -1 | 194.0, 249.4 | 6, 10 |
| 5 | -1 | -1 | +1 | -1 | 88.9, 106.1 | 15, 25 |
| 6 | +1 | -1 | +1 | -1 | 172.7, 160.1 | 13, 15 |
| 7 | -1 | +1 | +1 | -1 | 154.9, 182.2 | 17, 14 |
| 8 | +1 | +1 | +1 | -1 | 144.1, 162.4 | 14, 13 |
| 9 | -1 | -1 | -1 | +1 | 136.1, 107.0 | 17, 14 |
| 10 | +1 | -1 | -1 | +1 | 65.7, 60.0 | 10, 8 |
| 11 | -1 | +1 | -1 | +1 | 129.8, 107.2 | 11, 15 |
| 12 | +1 | +1 | -1 | +1 | 80.6, 87.7 | 9, 11 |
| 13 | -1 | -1 | +1 | +1 | 175.8, 164.8 | 19, 15 |
| 14 | +1 | -1 | +1 | +1 | 167.2, 166.1 | 13, 12 |
| 15 | -1 | +1 | +1 | +1 | 141.8, 129.2 | 14, 19 |
| 16 | +1 | +1 | +1 | +1 | 145.0, 140.1 | 13, 12 |

[a]At stress of 15 ksi (103 $MN/m^2$) and temperature of $1850^o$ F $(1010^o$ C).

TABLE IV. - Concluded.  SECOND FACTORIAL

EXPERIMENT, FULL REPLICATE OF $2^4$

(c) Coefficient estimates

| Coefficient | Estimate | Coefficient | Estimate |
|---|---|---|---|
| $\beta_{CAl}$ | 0.077 | $\beta_{TiC}$ | 0.024 |
| $\beta_{Al}$ | -.063 | $\beta_{CrAl}$ | -.021 |
| $\beta_{TiAl}$ | -.054 | $\beta_{Cr}$ | .015 |
| $\beta_{TiCAl}$ | .031 | $\beta_{TiCrCAl}$ | .013 |
| $\beta_{C}$ | .031 | $\beta_{CrC}$ | -.011 |
| $\beta_{TiCrC}$ | -.026 | $\beta_{TiCr}$ | -.004 |
| $\beta_{TiCrAl}$ | .025 | $\beta_{Ti}$ | .002 |
| $\beta_{CrCAl}$ | -.025 | | |

cessive.  Furthermore, if any kind of a statistical decision procedure is to be used to judge the adequacy of the first-degree model, we believe that at least 16 compositions should be used.  (The procedures of ref. 16 have been developed for experiments of 16, 32, or 64 treatments.)  Finally the full-factorial experiment (16 treatments) allows estimation of all possible interaction coefficients whereas a one-half replicate experiment could not estimate all of the two-factor interactions.

The compositions cast and the stress-rupture results obtained for the second factorial experiment are given in table IV(b).  Note the generally higher lives achieved here in comparison to those obtained in the first-factorial experiment (table II(b)).  This confirms the effectiveness of the steepest ascent operation seen in figure 7 and table III.

In the same manner as the first experiment the coefficient estimates of the second experiment were calculated by the Yates method.  These are tabulated in order of decreasing absolute effect in table IV(c).  In comparing these estimates with those of the first factorial experiment (fig. 6), the effects are generally lower in magnitude.  In fact, a chain-pooling analysis according to the method of reference 16 indicated that none of the effects in table IV(c) were significant (see appendix B).  This said that our response surface in hyperspace was nearly horizontal and, perhaps, our experiment was in the general vicinity of the maximum.  For such a situation the simple first-degree model is no longer adequate.

To summarize the Box-Wilson procedure so far in relation to the diagram of figure 2, the experimenting consisted of one experiment for a first-order model that was concluded to be adequate, followed by the exploration of the vector of steepest ascent for a new design center.  The second experiment for a first-order model led to the conclusion that the first-order model was not adequate and that the procedure then had to pass (see fig. 2) from the method of steepest ascents to the method of local exploration.

Local exploration. - The results of the second factorial experiment gave no clear-cut vector of ascent. Therefore, we concluded that there was no reason to shift the design center. The next step then was to determine the coefficients of a second-order equation of the form of equation (1), where $g = 4$ factors in this case. To do this, the factorial experiment was augmented with data from a set of center points and star points.

Each pair of star points was obtained by holding three of the four variables at the level of the design center 0 and varying the fourth variable. The levels $\rho_s$ suitable for such experimentation are tabulated in reference 17. According to reference 17, the levels for the variable not held fixed in this experiment should be two design units above and below the design center (+2 and -2). Thus, for the four-factor case here, a full set of star points consisted of $2 \times 4 = 8$ compositions. As the name implies, a set of star points form a star in hyperspace (centered around the design center), whereas the set of factorial points form the corners of a cube. This is shown for three-dimensional space in figure 8.

Along with the castings for the star points, four duplicate castings were made at the design center. The use of more than one center point serves two purposes. First, such points give a direct measure of the melt-to-melt scatter. Second, they are particularly effective in reducing the prediction error of the polynomial regression equation over the entire range of experimentation. This subject together with a discussion of the optimal
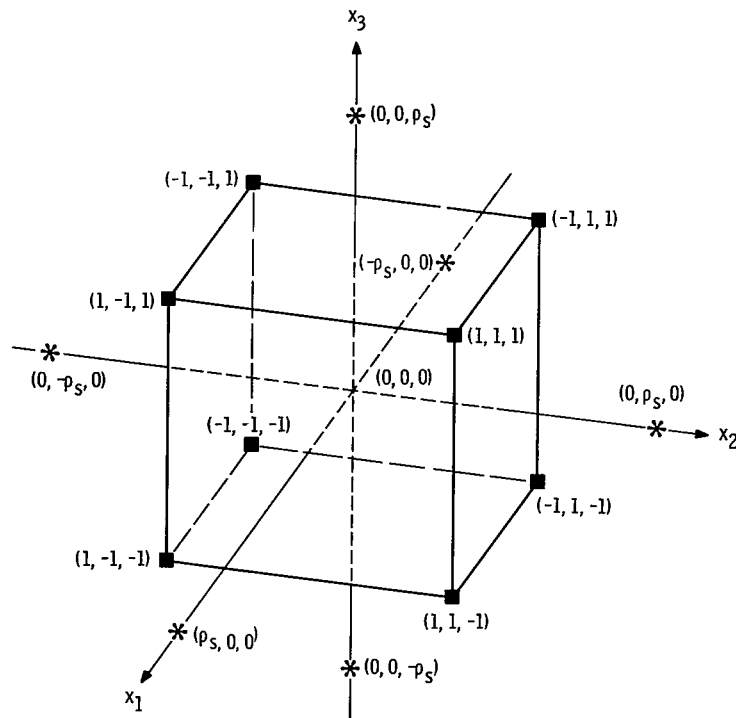


Figure 8. - Cube and star designs. ($\rho_s$ is distance of star points from design center.)

TABLE V. - STAR AND CENTER POINTS

| Alloy | Levels | | | | Stress-rupture[a] life, hr | Elongation,[a] % |
|-------|--------|--------|-------|--------|----------------------------|------------------|
|       | $x_{Ti}$ | $x_{Cr}$ | $x_C$ | $x_{Al}$ |                          |                  |
| S-1   | -2     | 0      | 0     | 0      | 108.6, 159.0               | 14, 13           |
| S-2   | +2     | 0      | 0     | 0      | 94.4, 95.6                 | 8, 8             |
| S-3   | 0      | -2     | 0     | 0      | 180.3, 186.6               | 15, 18           |
| S-4   | 0      | +2     | 0     | 0      | 219.5, 184.4               | 13, 12           |
| S-5   | 0      | 0      | -2    | 0      | 189.2, 150.0               | 8, (b)           |
| S-6   | 0      | 0.     | +2    | 0      | 220.3, 218.7               | 24, 14           |
| S-7   | 0      | 0      | 0     | -2     | 139.8, 123.4               | 19, 15           |
| S-8   | 0      | 0      | 0     | +2     | 153.1, 149.4               | 13, 14           |
| C-1   | 0      | 0      | 0     | 0      | 279.3, 269.7               | 13, 12           |
| C-2   | 0      | 0      | 0     | 0      | 198.4, 172.1               | 14, 11           |
| C-3   | 0      | 0      | 0     | 0      | 233.6, 203.9               | 12, 15           |
| C-4   | 0      | 0      | 0     | 0      | 242.8, 227.3               | 16, 11           |

[a]At stress of 15 ksi (103 $MN/m^2$) and temperature of 1850° F (1010° C).

[b]Fracture damaged; elongation not measurable.

number of center points is contained in reference 17. The levels used in this program, along with the corresponding stress-rupture results, are given in table V.

A regression equation of the form of equation (1) was fitted to all of the stress-rupture data in tables IV(b) and V by the least squares technique. The resultant expression was

$$\log t = 2.354 - 0.011\,x_{Ti} + 0.013\,x_{Cr} + 0.030\,x_C - 0.037\,x_{Al} - 0.085\,x_{Ti}^2 - 0.026\,x_{Cr}^2 - 0.026\,x_C^2 - 0.060\,x_{Al}^2$$

$$- 0.004\,x_{Ti}x_{Cr} + 0.025\,x_{Ti}x_C - 0.054\,x_{Ti}x_{Al} - 0.011\,x_{Cr}x_C - 0.021\,x_{Cr}x_{Al} + 0.077\,x_Cx_{Al} \tag{5}$$

where t is stress-rupture life in hours and the variables $x_{Ti}$, $x_{Cr}$, $x_C$, and $x_{Al}$ are in design units.

Equation (5) gives us the log of the rupture life as a function of composition. For a given composition it predicts the approximate life. It should be emphasized here that this equation should be used only within the limits of the experimentation, namely a sphere with a radius of 2 design units.

The next major step in the process is to characterize equation (5) geometrically and in particular to determine whether it has a maximum. This is done by the method of canonical reduction (ref. 10). This analysis can be rather involved mathematically;

therefore, only a brief summary of the main points are presented at this time. The details of the canonical reduction of equation (5) are given in appendix D.

Before the method of canonical reduction can be applied it is necessary to find the stationary point or point of zero-slope. It was found by differentiating equation (5) with respect to each variable and setting the derivatives equal to zero. This gave four equations in four unknowns ($x_{Ti}$, $x_{Cr}$, $x_C$, and $x_{Al}$). The simultaneous solution of these is the stationary point. The solution is given in table VI(a) in terms of both design units and natural units. This composition was given the designation NASA-SP.

The next question to be answered was, does this stationary point represent a true maximum or is it merely a saddle point or even a minimum? This is answered by the canonical reduction procedure. Without going into mathematical detail (see appendix D), a transformation of coordinate axes is made from the Cartesian system of the single elements to a Cartesian system that is symmetrical with the actual response surface (in hyperspace) and has its origin at the stationary point. If the stationary point is a true maximum, all paths from this new origin will result in decreased response. Performing a canonical reduction of equation (5) showed us that the stationary point was on a ridge, the stress-rupture life decreasing on all axes of symmetry except one where it remained es-

TABLE VI. - STATIONARY POINT

(a) Composition

[Contents of Ni, W, and Zr constant at 38, 14, and 0.25 wt. % respectively; balance, Co.]

| Element | Composition | |
|---------|-------------|-----|
| | Design units | Wt. % |
| Ti | +0.021 | 1.01 |
| Cr | +.215 | 2.11 |
| C | +.378 | .54 |
| Al | -.110 | 6.72 |

(b) Results of stress-rupture tests at 1850° F and 15 ksi (1010° C and 103 MN/m$^2$)

| Heat | Stress-rupture life, hr | Elongation, % |
|------|-------------------------|---------------|
| SP-1 | 186.0, 203.3 | 13, 14 |
| SP-2 | 203.7, 196.2 | 13, 16 |

sentially constant. Thus, for all practical purposes, we considered the stationary point essentially the optimum alloy with respect to stress-rupture life. This concluded the use of the Box-Wilson strategy.

The improvement of a second dependent variable (namely, the elongation) for essentially constant values of the primary independent variable (the stress rupture life) is discussed in appendix E.

Test results for the stationary point alloy. - Two castings of the stationary point alloy, NASA-SP, were made and tested at the standard stress-rupture conditions. The results are given in table VI(b). For the four tests made the average life was about 200 hours. Now, if we compare the composition of the stationary point alloy (table VI(a)) with that of the design center for the second factorial experiment (table IV(a)), we will find only slight differences; that is, the stationary-point alloy is very close to the design center. This suggests that the stress-rupture lives obtained for the design center (table V) should be similar to that of NASA-SP. The average of the lives for the design center was slightly higher (228 hr) than the stationary point alloy (197 hr). This is not too surprising, however, because the scatter of the design center data was fairly large (minimum of 172 hr to maximum of 279 hr). All the data points from NASA-SP fall within this range. Thus, we concluded the two compositions have essentially the same lives within the scatter. Furthermore, an analysis of variance (appendix F) led to the same conclusion.

In summary it may be said that prior to the Box-Wilson experimentation, the best experimental composition was GP-2 (maximum point of fig. 5). The starting point of the Box-Wilson strategy was elected to be a departure from that composition and the first factorial experiment and subsequent vector experiment forced a return to a composition that approximated that of the maximum point of figure 5. Subsequent experimentation according to the method of local exploration then showed (clearly and reliably for the first time) that not much additional improvement could be expected from further experimentation within the general composition region first established by the preliminary survey. Thus, only in retrospect, do we see that the maximum point of figure 5 would have been sufficient. However, one advantage of the stationary point alloy over GP-2 is that the response is relatively horizontal in the region of its composition so that wider tolerances in composition can be allowed in a specification of the stationary point alloy.

General remarks on the overall Box-Wilson process. - For the most part, the Box-Wilson process behaved as it theoretically should have: (1) The first factorial experiment indicated a clear vector of steepest ascent; (2) following this vector gave an increase in stress-rupture life to a maximum; (3) local exploration around the indicated vicinity of the maximum led to essentially an optimum with respect to the Ti, Cr, C, and Al content.

Strictly speaking, the optimization process is really not yet complete. We should have to consider the levels of all seven independent elements including Ni, W, and Zr.

Again, to limit the number of required castings, we simplified the process by neglecting these three elements. Our intent was to determine whether the Box-Wilson strategy of optimum seeking was useful in the optimization of alloy compositions. On the basis of this study, we feel that it does have clear and immediate value.

## Characterization of Stationary Point Alloy

Although the alloy was optimized only with regard to the stress-rupture life, we performed a minimal evaluation of several other properties of interest for gas turbine and other aerospace applications. These included as-cast mechanical properties, oxidation resistance, and microstructure.

Melting behavior. - All the material for the characterization of this alloy was produced by the vacuum induction melting procedure given earlier and using a 2900$^\circ$ F (1593$^\circ$ C) pour temperature. A typical macroetched stress-rupture specimen of NASA-SP is shown in figure 9.

Systematic deviations from the original charge composition occurred during the melting sequence. These are shown by table VII, which compares the chemical analyses of three randomly chosen heats with the charge composition. The retained tungsten con-



1 cm
0.5 in.
C-69-2431
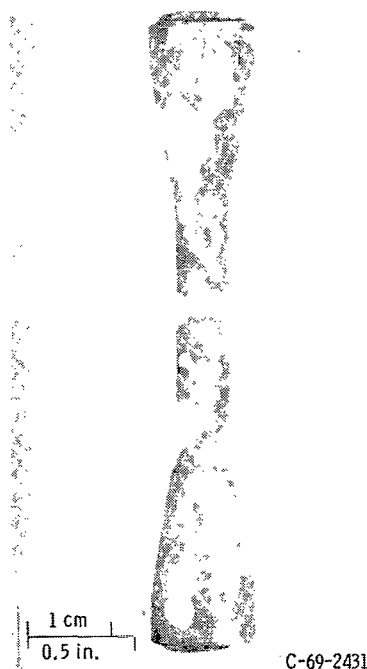
Figure 9. - As-cast stress-rupture specimen of alloy NASA-SP, macroetched to show typical surface grain size.

28

TABLE VII. - CHEMICAL ANALYSES OF

THREE RANDOMLY SELECTED

HEATS OF ALLOY NASA-SP

| Element | Charge composition, wt. % | Heat analyses, wt. % | | |
|---------|---------------------------|-------|-------|-------|
| Co | 37.37 | 37.65 | 38.05 | 37.61 |
| Ni | 38.00 | 37.99 | 38.03 | 38.03 |
| W | 14.00 | 13.89 | 13.70 | 13.83 |
| Al | 6.72 | 6.54 | 6.55 | 6.45 |
| Cr | 2.11 | 2.03 | 2.03 | 2.03 |
| Ti | 1.01 | .95 | .96 | .97 |
| Zr | .25 | .39 | .33 | .50 |
| C | .54 | .47 | .48 | .45 |

tent was slightly, but consistently, lower than the charge composition. Aluminum and chromium were consistently low because of their high vapor pressures. Carbon was lower than the charge level because of the carbon boil; that is, carbon is pumped off in the form of CO during deoxidation of the melt by the reaction $C + O \rightarrow CO$. Possibly the carbon boil was maintained too long because the zirconium content was consistently high, indicating some reduction of the $ZrO_2$ crucible. All of these mentioned deviations from the charge composition were extremely consistent, indicating reproducibility of the melting procedure. Because these deviations from the charge composition may be of some importance to the stress-rupture properties, the retained composition (table VII) should be considered the aim. The average of these compositions is approximately 37.8Co-38.0Ni-13.8W-6.5Al-2.0Cr-1.0Ti-0.4Zr-0.47C.

Physical properties. - The density of NASA-SP was measured at 0.307 pound mass per cubic inch (8.51 g/cm$^3$). This represents an average of two determinations from different heats. The alloy was also observed to be weakly ferromagnetic at room temperature.

Mechanical properties. - Stress-rupture data were obtained at 1500°, 1700°, 1850°, and 2000° F (816°, 927°, 1010°, and 1093° C). These are tabulated in table VIII and are plotted in figure 10. The isothermal curves of figure 10 were crossplotted at 100 and 1000 hours to obtain the isochronal curves of figure 11. These curves are compared with the range of data for commercial cast Ni- and Co-base superalloys (ref. 18). One observes the following:

(1) NASA-SP is stronger in stress-rupture than commercial cast Co-base alloys up to about 1825° F (996° C). Increasing temperature leads to a more rapid loss in strength than that for the carbide strengthened Co-base alloys, so that a crossover occurs above

TABLE VIII. - SUMMARY OF STRESS-RUPTURE

DATA FOR ALLOY NASA-SP

| Temperature | | Stress | | Life, hr | Elongation, % |
|---|---|---|---|---|---|
| °F | °C | ksi | MN/m² | | |
| 1500 | 816 | 70 | 483 | 10.0 | 2 |
| | | 70 | 483 | 10.9 | 2 |
| | | 60 | 414 | 79.3 | 2 |
| | | 60 | 414 | 97.5 | 2 |
| | | 50 | 345 | 250.6 | 1 |
| | | 50 | 345 | 356.7 | 2 |
| | | 50 | 345 | 364.4 | 2 |
| | | 40 | 276 | 1683.6 | 1 |
| | | 40 | 276 | 1996.2 | 3 |
| 1700 | 927 | 40 | 276 | 11.9 | 4 |
| | | 40 | 276 | 13.5 | 2 |
| | | 35 | 241 | 43.9 | 4 |
| | | 35 | 241 | 50.0 | 4 |
| | | 30 | 207 | 148.2 | 4 |
| | | 30 | 207 | 163.4 | 2 |
| | | 25 | 172 | 344.1 | 5 |
| | | 25 | 172 | 360.6 | 6 |
| | | 25 | 172 | 385.3 | 6 |
| | | 25 | 172 | 404.6 | 6 |
| | | 20 | 138 | 1132.6 | 7 |
| | | 20 | 138 | 1209.4 | 7 |
| 1850 | 1010 | 25 | 172 | 6.5 | 10 |
| | | 25 | 172 | 9.1 | 9 |
| | | 20 | 138 | 31.5 | 12 |
| | | 20 | 138 | 34.4 | 17 |
| | | 20 | 138 | 37.6 | 13 |
| | | 15 | 103 | 186.0 | 13 |
| | | 15 | 103 | 196.2 | 16 |
| | | 15 | 103 | 203.3 | 14 |
| | | 15 | 103 | 203.7 | 13 |
| | | 10 | 69 | 725.2 | 9 |
| | | 10 | 69 | 1275.1 | 22 |
| | | 10 | 69 | 1449.7 | 23 |
| 2000 | 1093 | 10 | 69 | 5.1 | 39 |
| | | 10 | 69 | 8.5 | 30 |
| | | 7.5 | 52 | 49.7 | 40 |
| | | 7.5 | 52 | 63.7 | 33 |
| | | 5 | 34 | 481.8 | 37 |
| | | 5 | 34 | 562.3 | 38 |
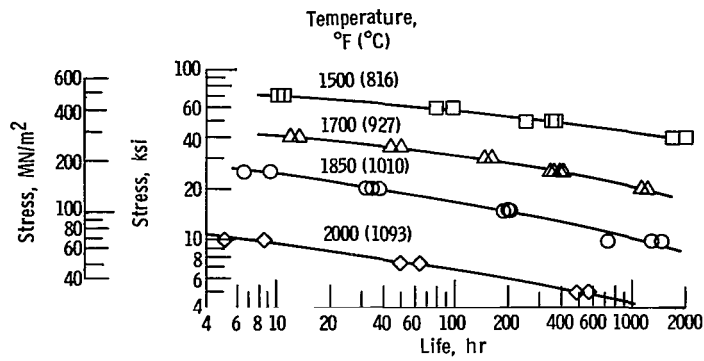
Figure 10. - Isothermal stress-rupture curves for alloy NASA-SP.



(a) 100-hour life.

(b) 1000-hour life.
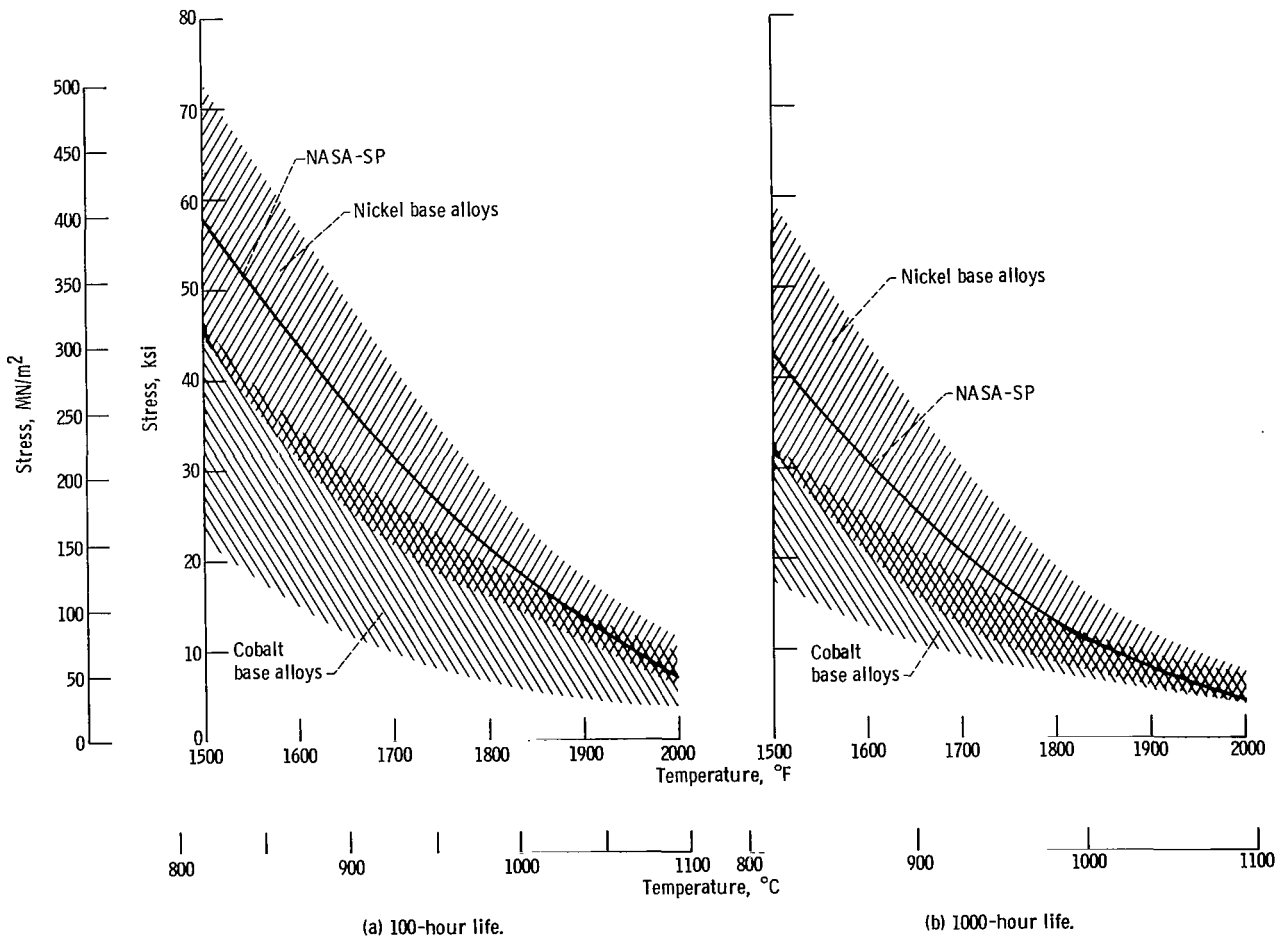
Figure 11. - Isochronal stress-rupture curves for alloy NASA-SP compared with commercial cast nickel and cobalt base alloys (ref. 18).

1825° F (996° C). This is apparently a result of the rapid coarsening and dissolution of the strengthening gamma-prime phase with increasing temperature.

(2) NASA-SP has lower stress-rupture capability than the better commercial cast Ni-base alloys. It has approximately 100° F (56° C) lower use temperature than the best of the Ni-base alloys.

The stress-rupture elongations (table VIII) were quite high at the higher temperatures (up to 40 percent at 2000° F (1093° C)). However, elongations were very low (1 to 3 percent) at 1500° F (816° C). No attempt has been made to improve the low temperature ductility by heat treatment.

A few creep curves were obtained. These are shown in figure 12. Figure 12(a) shows a curve obtained at 1500° F (816° C) and 50 ksi (345 MN/m$^2$) initial stress. There



(a) Stress, 50 ksi (345 MN/m$^2$); temperature, 1500° F (816° C).

(b) Stress, 25 ksi (172 MN/m$^2$); temperature, 1700° F (927° C).
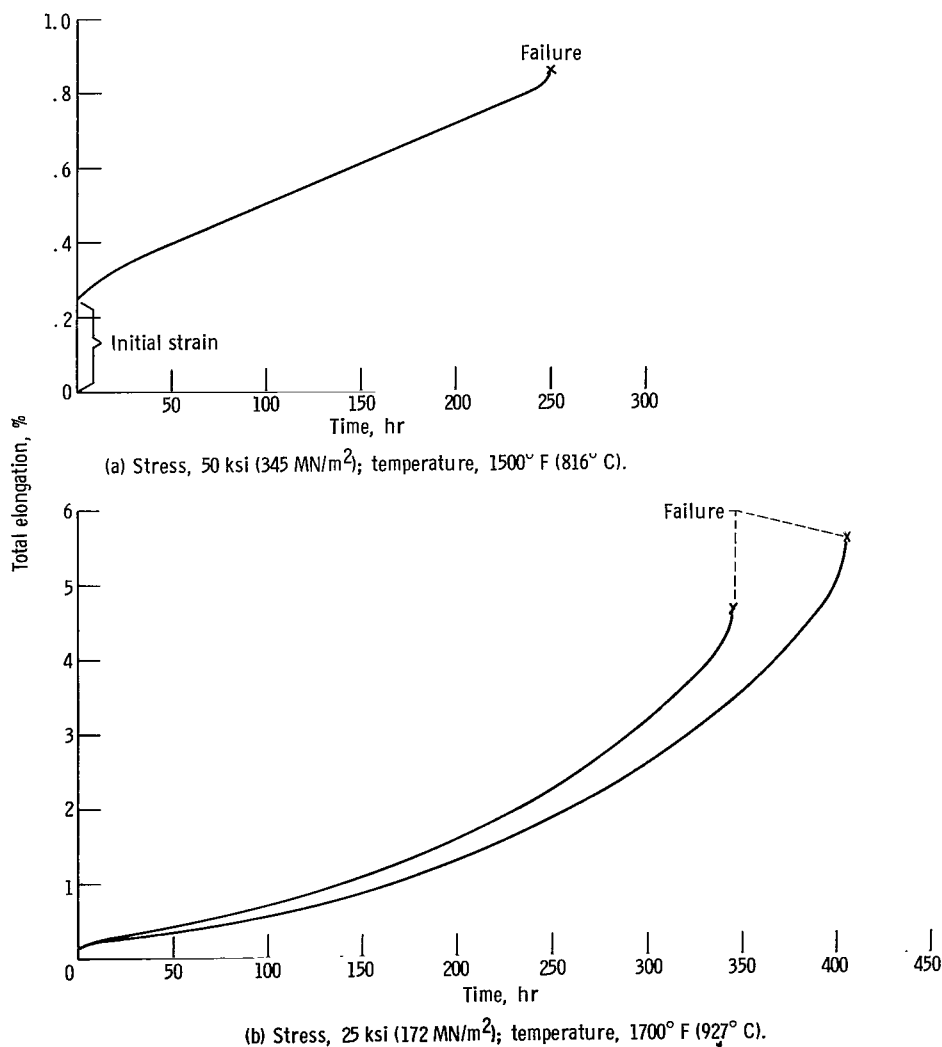
Figure 12. - Creep curves for alloy NASA-SP.

was a short first stage followed by a very long linear portion and an extremely short third stage just prior to failure. Again note the low elongation at fracture. In contrast to this, figure 12(b) shows two curves obtained from tests run at 1700° F (927° C) and 25 ksi (172 MN/m$^2$) where much more elongation occurred before failure. Here, little first- and second-stage creep occurred, and the curves show essentially all third-stage behavior. The two curves shown in figure 12(b) represent specimens from two heats. We consider the degree of reproducibility to be fairly good for cast materials.

The tensile properties of NASA-SP as a function of temperature are shown in figure 13. Ultimate tensile strength remained approximately constant at 100 ksi (689 MN/m$^2$) up to a temperature of about 1500° F (816° C). Above this temperature, the tensile strength showed a uniform decrease. Corresponding to this decrease was an increase in elongation. Comparing these data with the curves of reference 19, we find that the ten-
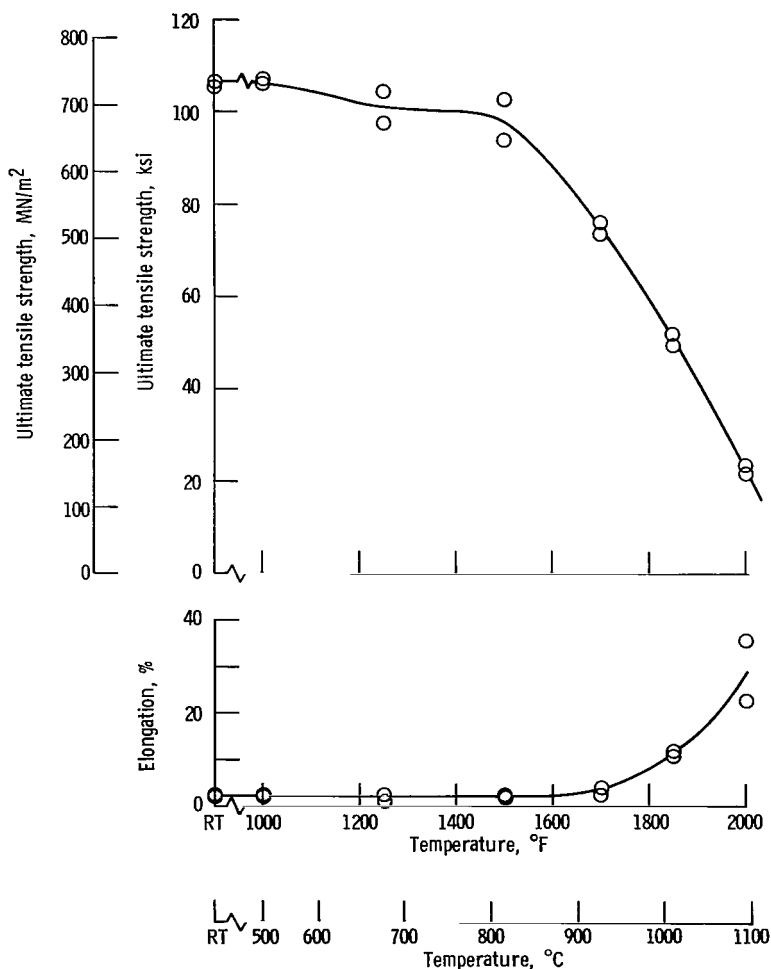


Figure 13. - Tensile properties of alloy NASA-SP as function of test temperature. (RT denotes room temperature.)

sile strength of NASA-SP is generally higher than the cast commercial Co-base alloys above 1400° F (760° C) but well below the strength levels of the best commercial Ni-base alloys. The low temperature ductility is generally lower than that of either Co- or Ni-base alloys. However, ductility increases with temperature from about 2 percent at 1500° F (816° C) to about 30 percent at 2000° F (1093° C).

Oxidation. - A limited number of cyclic oxidation tests were run on NASA-SP both in static air and in the combustion products of the Mach 1 gas burner. This gave some indication as to how the alloy ranked with respect to some commonly used commercial alloys.
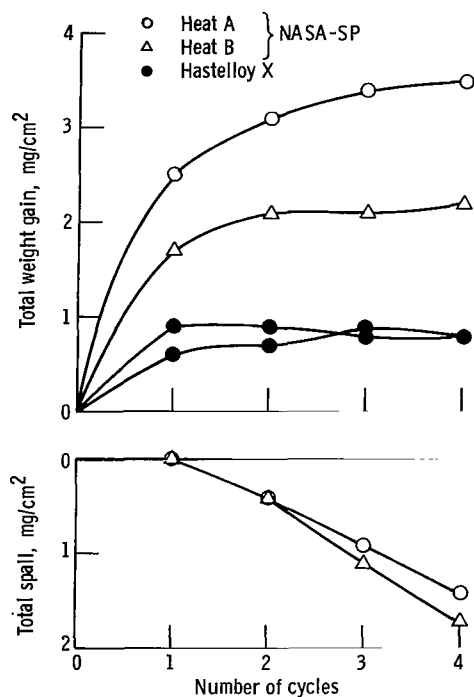


Figure 14. - Results of cyclic oxidation tests run in static air. Cycle: 100 hours at 1800° F (982° C) followed by approximately 15-minute cool to room temperature.

Figure 14 shows the results of test run in static air with 1800° F (982° C), 100-hour cycles. The two curves for NASA-SP represent specimens from two heats. Two Hastelloy X specimens (taken from commercial bar stock) were run at the same time for comparison. Using weight gain as a measure, NASA-SP was somewhat lower in oxidation resistance than Hastelloy X. However, considering the low chromium content of NASA-SP, the oxidation resistance was comparatively good, suggesting a beneficial effect of Al. The lower oxidation resistance of NASA-SP in comparison to Hastelloy X was partly due to the fact that the NASA-SP began to spall at the end of the second cycle. Hastelloy X did not spall.

The results of cyclic tests in the high velocity burner rig up to a maximum cycle temperature of 2000° F (1093° C) are shown in figure 15. The data for NASA-SP are shown along with results for commercial IN 100 and X-40 (HS-31), which are essentially the most oxidation resistant cast Ni- and Co-base alloys, and MarM 200 and WI-52, which are essentially the least oxidation resistant Ni- and Co-base alloys tested to date in the apparatus (ref. 12). The weight-loss points plotted represent the average from five to seven wedge-shaped specimens (see fig. 3). Weight is lost rather than gained because of loss of the oxide spall during the cooling portion of the cycle and perhaps also as a result of oxide evaporation and erosion at temperature. Although NASA-SP was inferior to the Ni-base alloy IN 100, it was nearly as resistant to oxidation and erosion as the high-chromium (25 percent) Co-base alloy X-40 and the Ni-base alloy MarM 200. It was much superior to the Co-base alloy WI-52.

Thermal fatigue cracking data are shown in figure 15(b). NASA-SP was less prone to cracking than the two Ni-base alloys IN 100 and MarM 200 but somewhat more prone than the Co-base alloys X-40 and WI-52.

X-ray diffraction was used to identify the oxidation products formed on NASA-SP in both static and high-velocity oxidation tests. Scrapings from a specimen oxidized in static air for 400 hours at 1800° F (982° C) showed two oxide phases adhering to the surface: (1) a monoxide (MO) of lattice parameter $a_o \cong 4.23$ Å ($4.23 \times 10^{-10}$ m), which lies between the values for NiO and CoO and (2) a tungstate phase, whose d-values correspond approximately to $CoWO_4$. Spall that fell from this specimen during cooling was also checked by X-ray diffraction. This again showed MO ($a_o \cong 4.23$ Å) and a tungstate phase which corresponded slightly more closely in d-values to $NiWO_4$.

Scrapings from a sample run in dynamic oxidation for 100 hours at 2000° F (1093° C) showed two phases:
  (1) MO with lattice parameter $a_o \cong 4.22$ Å ($4.22 \times 10^{-10}$ m) (This phase was very loosely adherent.)
  (2) a spinel of lattice parameter $a_o \cong 8.11$ ($8.11 \times 10^{-10}$ m) corresponding fairly closely to $CoAl_2O_4$ (This phase had the blue color of the Co-Al spinel.)
It should be emphasized at this point that this represents a very incomplete picture
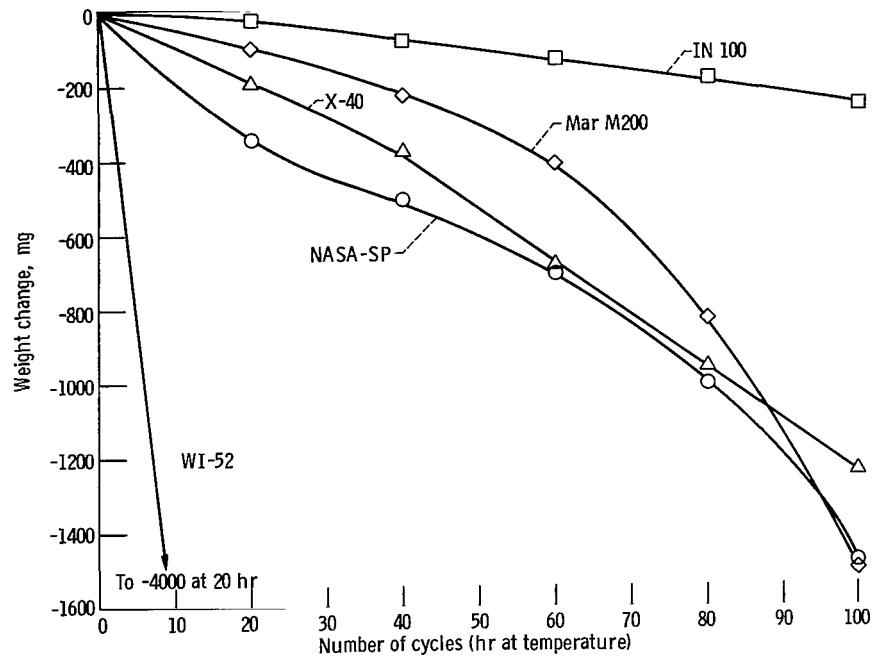
(a) Weight change.
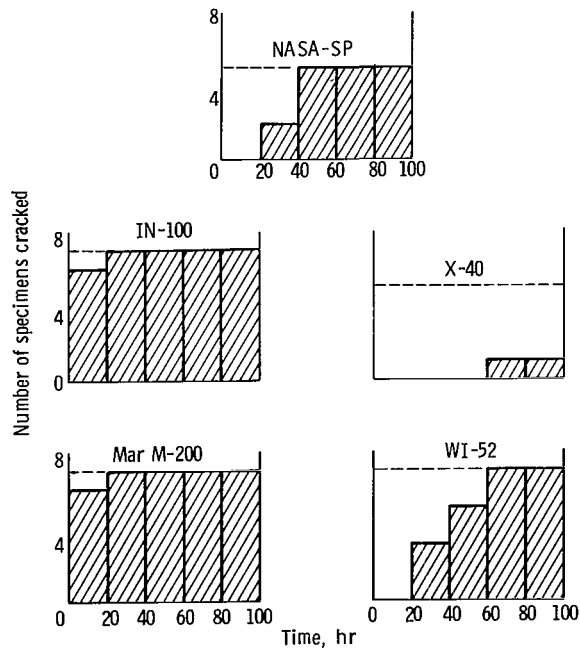


(b) Thermal fatigue cracking. (Dashed line denotes total number of specimens tested.)

Figure 15. – Results of cyclic oxidation tests run in Mach 1 gas burner stream. Cycle: 1 hour at 2000° F (1093° C) followed by approximately 1.5-minute cool to room temperature.

of the oxidation behavior of NASA-SP. A thorough study of the oxidation behavior has not been attempted. Furthermore, corrosion in a sulfur-salt atmosphere (perhaps a more critical test in view of the low Cr content) has not been evaluated.

Microstructure and phase identification. - The final alloy NASA-SP was studied in the as-cast form with the object of identifying the phases present in the microstructure. We made use of optical microscopy, replica electron microscopy, electron microprobe analysis, and X-ray diffraction. If correct, phase identifications with all of these techniques should be consistent. Therefore, all results are presented and discussed more or less simultaneously. The microstructure of NASA-SP is shown by optical micrographs in figure 16 and by a replica electron micrograph in figure 17. Figure 18 shows area scans made with the electron microprobe. X-ray images of the same area for each of the eight added elements are shown along with a back scattered electron image and a light micrograph of the same area (etched after the X-ray images were made). Finally, a summary of the X-ray diffraction data is given in table IX.

Before discussing the conclusions drawn from these observations, we would like to make a few remarks about the validity of the X-ray diffraction data from our electrolytic extractions (table IX). Although this method is absolutely necessary in many cases, the results must be considered with a good deal of caution. First of all, the detection of a plausible phase in the residue is usually a valid indication that that phase is present in the microstructure. However, the absence of evidence of a phase in a residue does not necessarily indicate its absence in the microstructure: (1) It may have been dissolved by the electrolyte, or (2) it may be enveloped by another phase which a soft radiation like $CrK_{\alpha}$ cannot penetrate. Possibility (2) was the observation made with TiC in as-cast NASA-SP. For these reasons, quantitative measures of the amounts of phases present are rather tenuous unless very precise control is maintained over the extraction conditions. We feel that the control here was not precise enough for quantitative results.

Finally two comments regarding our X-ray diffraction results in table IX:

(1) The use of stoichiometric symbols (i. e., TiC and ZrC) is made only for simplicity. As is well known and will be shown later by the microprobe results, other elements can undoubtedly substitute in these compositions.

(2) The strongest line of the gamma-prime phase was a rather broad diffuse line over which was superimposed another very sharp line. We interpreted this as the presence in the residue of two phases (gamma solid solution and gamma prime) of virtually the same lattice parameter, indicating that the extraction process did not completely dissolve the gamma matrix.

Returning to the metallurgy of NASA-SP, there are four main features in the optical micrographs (fig. 16):

(1) A matrix with a uniform dispersion of fine, optically irresolvable precipitate particles
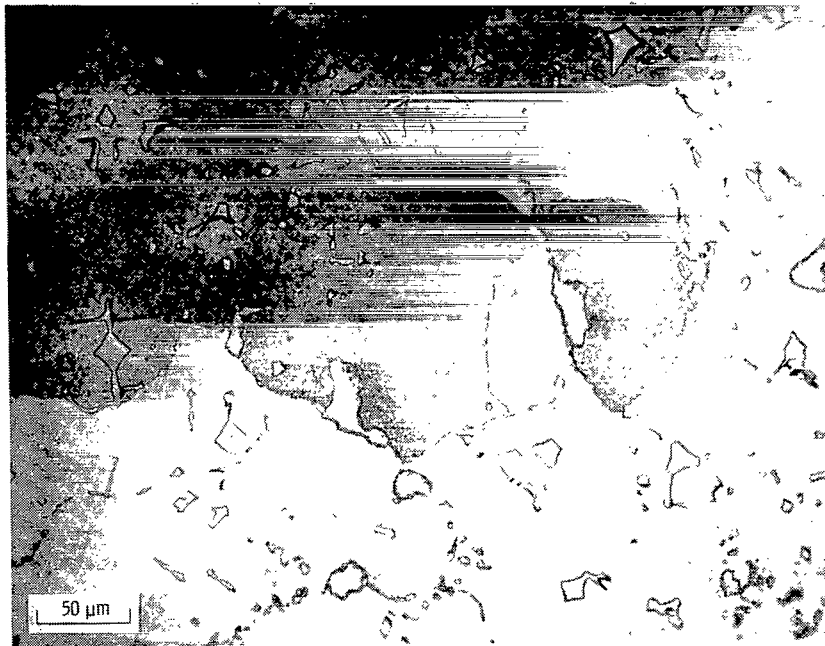
(a) Magnification, 250.
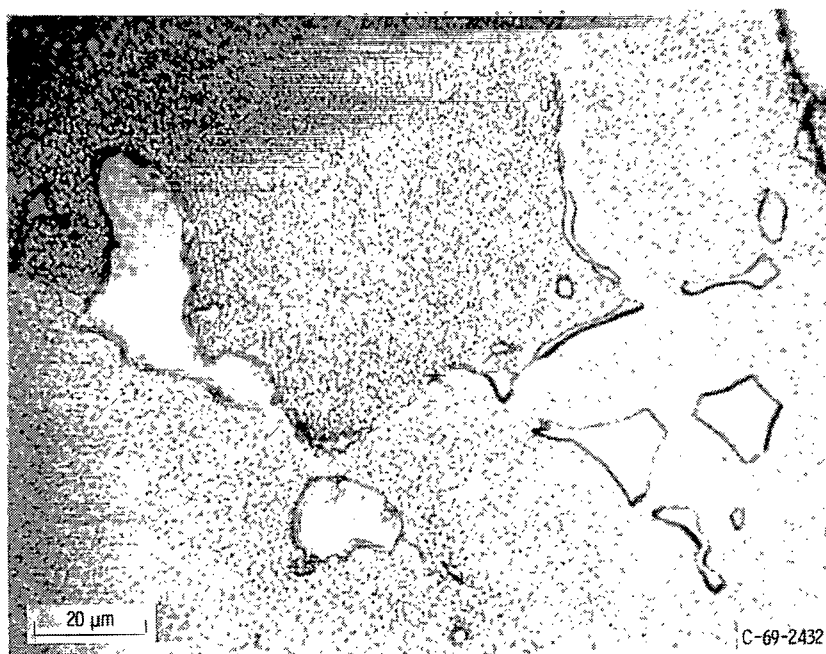


(b) Magnification, 750.

Figure 16. – As-cast microstructure of alloy NASA-SP by optical microscopy.

TABLE IX. - SUMMARY OF X-RAY DIFFRACTION DATA

ON EXTRACTED RESIDUE FROM ALLOY NASA-SP

[Cu $K_\alpha$ radiation.]

| Phase | Condition | | | |
|---|---|---|---|---|
| | As-cast | | Stress-rupture tested[a] | |
| | Intensity[b] | Lattice parameter, $a_o$, Å, (or $10^{-10}$ m) | Intensity[b] | Lattice parameter, $a_o$, Å, (or $10^{-10}$ m) |
| [c]$\gamma'$ | Strong | ~3.58 | Strong | ~3.58 |
| TiC | Weak | ~4.32 | Medium | ~4.31 |
| ZrC | ------ | ---- | Weak | ~4.63 |

[a]$1850^\circ$ F, 10 ksi, 1449.7 hr ($1010^\circ$ C, 69 MN/m$^2$).

[b]Relative intensities of the strongest lines, judged visually from the films.

[c]Some $\gamma$ solid solution believed to be present along with $\gamma'$.

(2) Large carbides (those particles on the right in fig. 16(b)), which incidentally could be seen in relief before etching

(3) Smaller, darker etching carbides (two small particles on extreme left of fig. 16(b)), which could also be seen before etching but did not stand in relief as much as the larger carbides

(4) Large intermetallic particles (on the left in fig. 16(b)), which were rapidly attacked by most etchants tried

The fine precipitate was easily resolved by electron microscopy (fig. 17). Its tendency toward cubic shape and orientation is typical of gamma prime precipitated in Ni-base alloys (ref. 14). Note also in figure 17 how the two intermetallic particles were heavily attacked by the etchant (Murakami's) in comparison to the carbide particle.

First, let us consider the large carbide phase. Particles of this phase are identified by A in figure 18(a). The X-ray diffraction data (table IX) clearly showed the presence of an MC with a lattice parameter very similar to TiC. The X-ray images (fig. 18) confirmed this, showing the presence of Ti and C in these particles (fig. 18(h) and (j)). Tungsten was also in the carbide particles (fig. 18(e)), supporting our earlier statement on substitution of other elements in the MC carbides. Except for W and perhaps a slight amount of Zr, however, other elements are largely absent in the carbide.

Second, consider the small carbide particles. Their positions are marked with B in figure 18(a) and coincided with the spots seen on the Zr X-ray image (fig. 18(i)). In fact, most of the Zr in the alloy appeared to be located in this phase, suggesting that it would
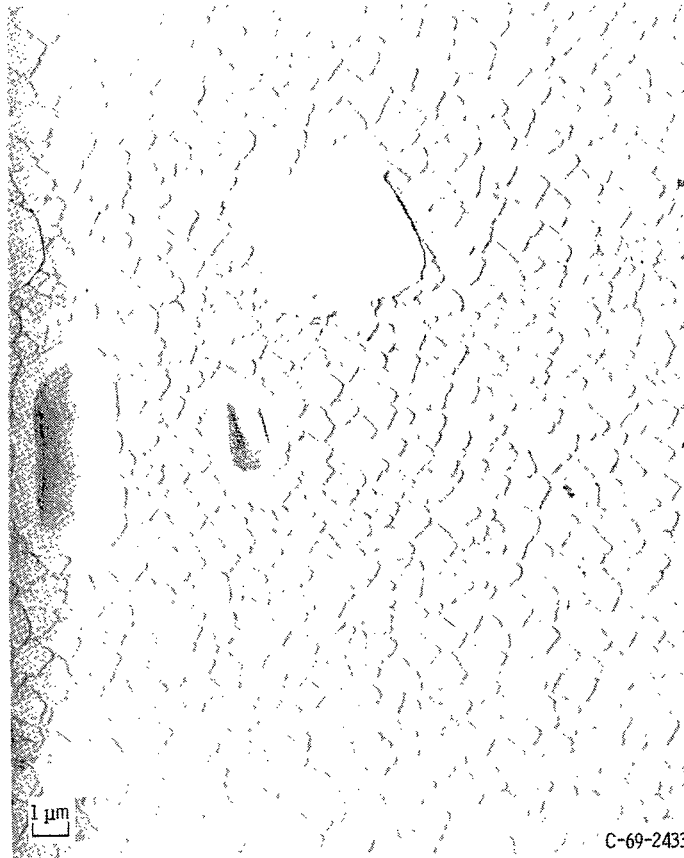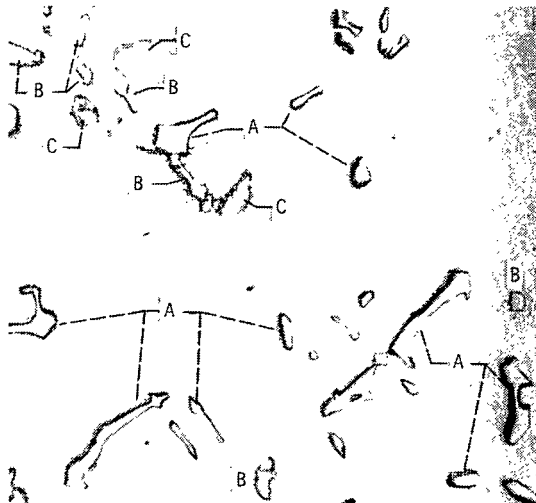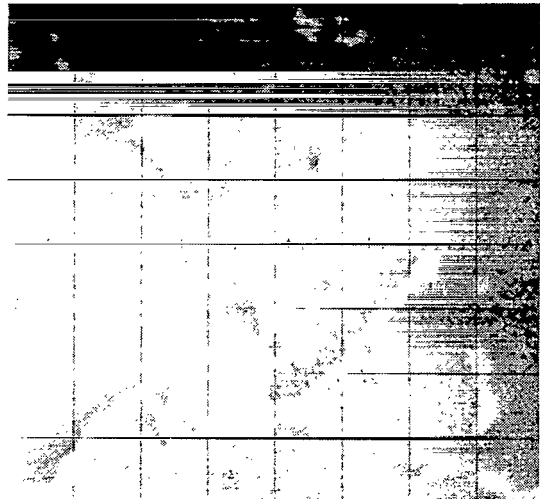
Figure 17. - As-cast microstrucutre of alloy NASA-SP by replica electron microscopy.
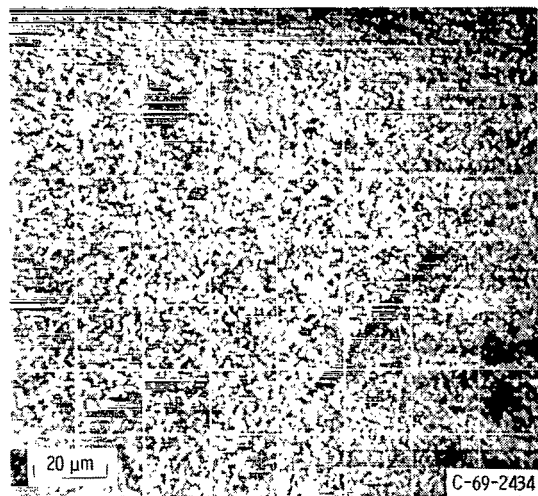
(a) Light micrograph. (A shows large carbides; B, small darker carbides; and C, intermetallic particles.)
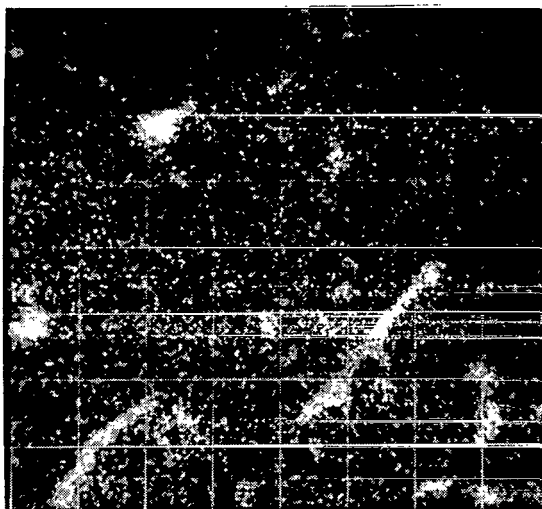
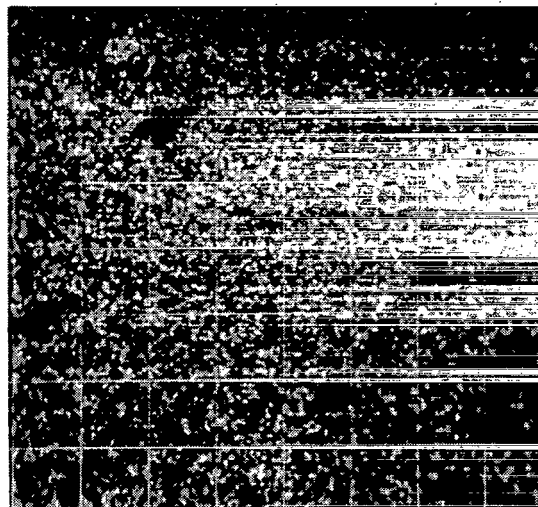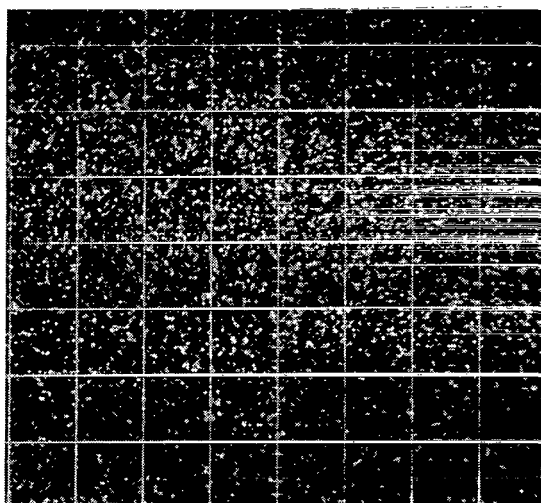(b) Back-scattered electrons

(c) Co K$_\alpha$

(d) Ni K$_\alpha$

20 μm

C-69-2434

Figure 18. – X-ray images obtained from as-cast specimen of alloy NASA-SP. X500.

(e) W M$_\alpha$

(f) Al K$_\alpha$

(g) Cr K$_\alpha$

(h) Ti K$_\alpha$

20 μm

C-69-2435
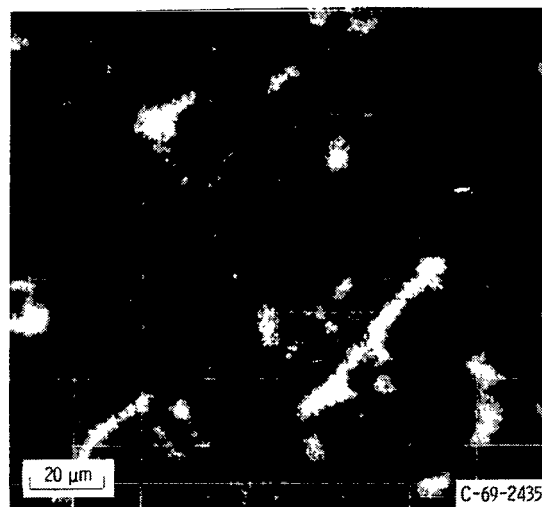
Figure 18. - Continued.
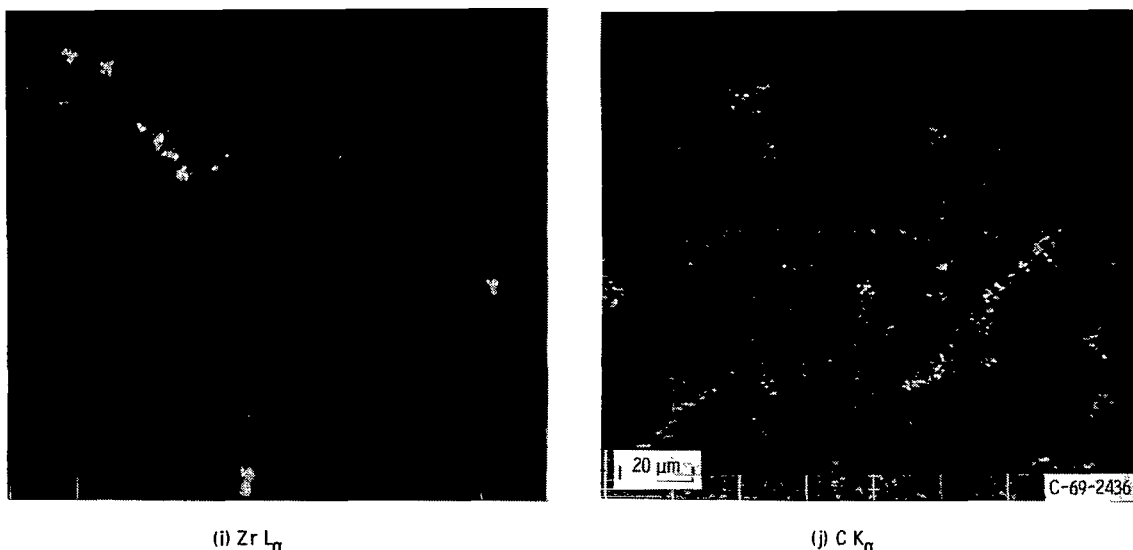
(i) Zr L$_\alpha$            (j) C K$_\alpha$

Figure 18. - Concluded.

have been better if we had also considered this element in the optimization of the alloy system. Cobalt, nickel, carbon, and small amounts of W and Ti were also present in the small carbides. This can just barely be seen in figure 18. It was shown somewhat better in higher magnification X-ray images that were taken but are not shown here. The X-ray diffraction studies (table IX) did not give any indication of any phases other than the gamma prime and TiC in as-cast NASA-SP. Thus we were not able to make a positive identification of this phase. However, based on its microstructural appearance, the presence of C, and the high concentration of Zr, we feel that this phase is probably a MC, nominally ZrC. Its apparent absence in the X-ray diffraction pattern of the extracted residue is presumably because of its relatively small amount. As will be mentioned later, the presence of ZrC was seen in residue from a tested stress-rupture specimen.

Third, consider the large intermetallic phase. There are three particles of this phase in the upper left quadrant of figure 18 (marked C in fig. 18(a)). Also the presence of these particles can be seen as dark spots in the back-scattered electron shot (fig. 18(b)). There is a higher concentration of Al in this phase than in the rest of the micro-structure. Also Ni and Co are present. It is somewhat surprising that a higher concentration of Cr was not found in this phase, because in the optimization portion of the program an increase in the amount of this intermetallic phase correlated with increased Cr content (and decreased stress-rupture life). Because of its tendency to be preferentially attacked by all etchants tried, it was apparently dissolved in the extraction process. As a result, no X-ray diffraction pattern of this phase was obtained. Thus, we cannot make positive identification of the intermetallic. We would speculate, however, that it is perhaps a beta-phase of the form (Ni, Co) Al.

Finally, consider the fine precipitate which we have presumed to be gamma-prime. Unfortunately, the particle size is too small to allow the use of the electron microprobe, at least on as-cast NASA-SP. However, we felt fairly confident that this is indeed gamma-prime on the basis of our X-ray diffraction results and its morphology.

What we have established is the nature of the as-cast microstructure. Of great importance to the high-temperature strength of any alloy is how its microstructure changes with prolonged high-temperature exposure, especially under stress. To obtain some indication of this in NASA-SP, the gage sections from long-time stress-rupture tests were metallographically examined. These are shown in figure 19 for all four test temperatures. In these photomicrographs the gamma-prime is the lighter phase. The darker areas then represent the gamma matrix which has been very finely mottled from gamma-prime precipitation during cooling from the test temperature. First, notice how the gamma-prime became much coarser, the higher the test temperature. This overaging process is undesirable from a strength standpoint. A second thing to notice (figs. 19(b) and (c)) is how interconnected the gamma-prime has become in comparison to the discrete particles observed in the as-cast alloy (fig. 17). At 2000$^{o}$ F (1093$^{o}$ C) some of the gamma-prime phase goes into solution, and the gamma-prime again takes the form of more or less discrete particles (fig. 19(d)).

A rather high volume fraction of gamma-prime is evident after coarsening. Even as-cast (fig. 17) the high volume fraction of gamma-prime is evident. At 2000$^{o}$ F (1093$^{o}$ C) some solutioning has occurred (fig. 19(d)). Also we can see some evidence of carbide solutioning at this temperature.

An observation was made regarding the unknown intermetallic phase. This can best be seen in figure 19(a), although the same effect was seen at other temperatures and test times. With high-temperature exposure the intermetallic particles decomposed into what appeared optically to be large islands of gamma-prime with a few small carbide particles. With longer time exposures at higher temperatures, the large gamma-prime regions become somewhat washed out in the general gamma-prime coarsening process. Associated with stress-rupture testing (at least at 1850$^{o}$ F (1010$^{o}$ C)) was the appearance of a second MC in the X-ray diffraction pattern that was not seen in the residue from the as-cast specimen (see table IX). This MC had a lattice parameter very close to that of ZrC.

On first glance, figure 19(b) might suggest the presence of a plate-like or needle-like phase similar to the sigma phase occasionally found in some Ni-base superalloys (ref. 14). On close examination, however, we concluded that these were not precipitates. Rather, they appear to be some sort of deformation bands, such as coarse slip or perhaps twinning. The density of these deformation bands increased near the fracture where the greatest amount of deformation had occurred. This structure was seen most clearly in the 1700$^{o}$ F (927$^{o}$ C) specimen (fig. 19(b)). Very faint ghosts of this could be seen with the 1850$^{o}$ F (1010$^{o}$ C) specimen. None were seen in the 1500$^{o}$ or 2000$^{o}$ F
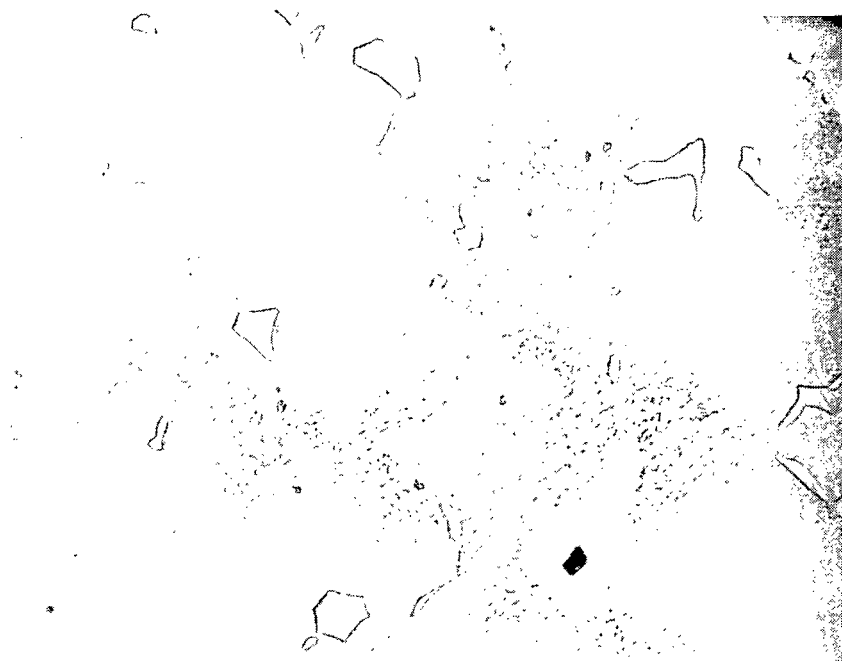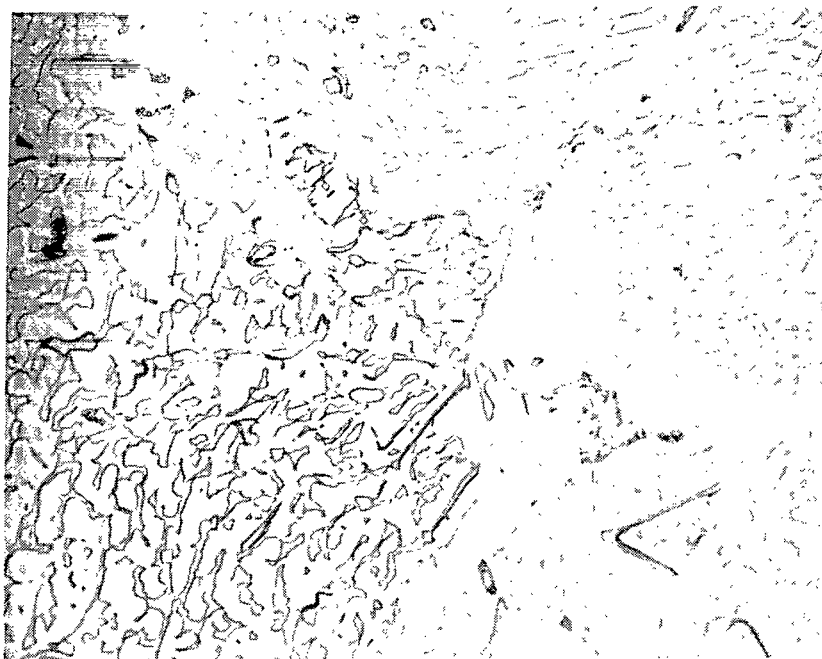
(a) Temperature, 1500° F (816° C); stress, 40 ksi (276 MN/m$^2$); time, 1683.6 hours.
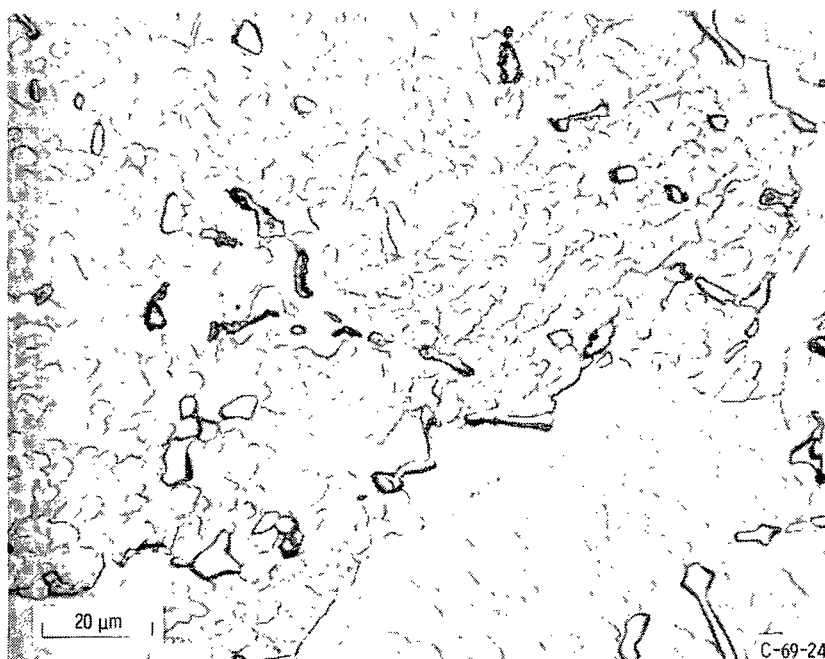


20 μm

C-69-2437
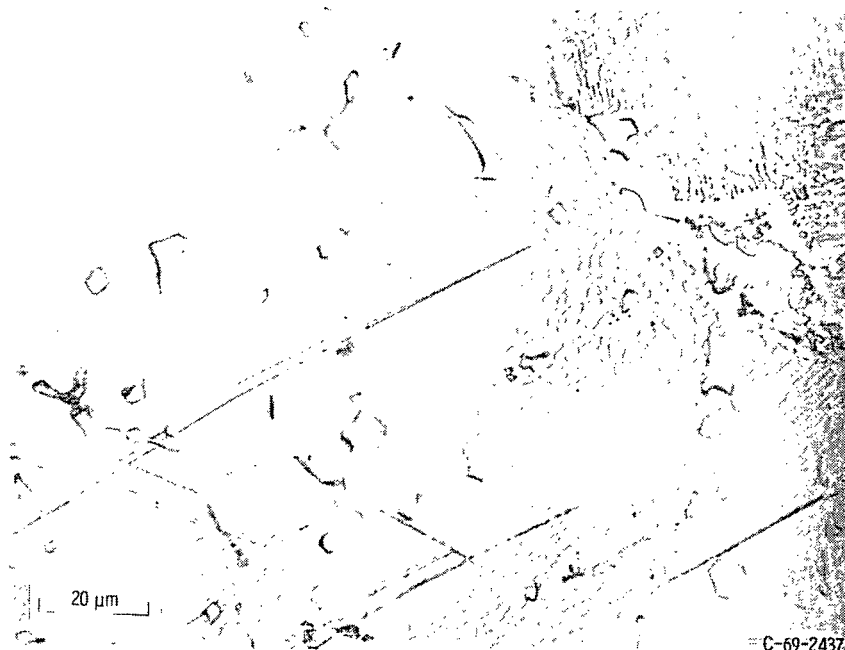
(b) Temperature, 1700° F (927° C); stress, 20 ksi (138 MN/m$^2$); time, 1132.6 hours.

Figure 19. - Microstructure of NASA-SP after long-time stress-rupture tests at various temperatures. Photomicrographs taken in stressed section on plane parallel to stress axis. X750.

(c) Temperature, 1850° F (1010° C); stress, 10 ksi (69 MN/m$^2$); time, 1275.1 hours.



(d) Temperature, 2000° F (1093° C); stress, 5 ksi (34 MN/m$^2$); time, 481.8 hours.

Figure 19. - Concluded.

($816^O$ or $1093^O$ C) specimens. Within the limits of our testing times and temperatures, no other metallographic evidence was seen that would suggest long-time embrittlement.

## CONCLUDING REMARKS

This program has successfully demonstrated two things:

(1) The usefulness of the Box-Wilson strategy for the optimization of an alloy composition. Although the scope was limited by optimizing only one condition of stress-rupture life among several possible dependent variables and by optimizing with respect to only four of the seven possible independent (composition) variables, we feel the potential for wider use of the strategy has been shown.

(2) The potential for a new gamma-prime-strengthened superalloy composition having applications in turbine engines and other aerospace devices requiring high-temperature properties. Although the alloy developed (NASA-SP) is inferior to the best cast Ni-base alloys, it is comparable to the best Co-base alloys. It represents a composition range not yet exploited in commercial superalloys, namely, the combination of low Cr, high Co, and gamma-prime strengthening.

## SUMMARY OF RESULTS

The following results were obtained from a program to develop a gamma-prime strengthened Co-Ni alloy using the Box-Wilson experimental strategy of optimum seeking:

1. A previously developed NASA Co-base alloy cobalt - 25 tungsten - 1 titanium - 0.5 zirconium - 3.12 chromium - 0.6 carbon (Co-25W-1Ti-0.5Zr-3.12Cr-0.6C; charge composition, wt. %) was modified by additions of Ni and Al. The resulting composition 38Co-38Ni-14W-0.5Ti-0.25Zr-1.75Cr-0.35C-7Al, developed a fine dispersion of gamma-prime precipitate and had stress-rupture strength promising enough to warrant further investigation.

2. The stress-rupture life at $1850^O$ F and 15 ksi ($1010^O$ C and 103 $MN/m^2$) was optimized with respect to the levels of Ti, Cr, C, and Al using the statistically founded Box-Wilson strategy of experimentation. A factorial experiment was performed, followed by a vector of steepest ascent, in turn, followed by another factorial experiment. This indicated the general region of a maximum in stress-rupture life. Further data (star and center points) allowed stress-rupture life to be expressed as a second-order polynomial function of composition. Canonical reduction of this equation indicated a family of compositions along a ridge of approximately constant stress-rupture life of approximately 200 hours. The stationary point alloy from this family of compositions was 37.4Co-38.0Ni-14.0W-6.72Al-2.11Cr-1.01Ti-0.25Zr-0.54C. This alloy was designated NASA-

SP and was further characterized to determine properties important to gas turbine and other high temperature aerospace devices.

3. Slight but systematic deviations occurred from the charge composition to the actual retained composition. The preferred retained composition of alloy NASA-SP is 37.8Co-38.0Ni-13.8W-6.5Al-2.0Cr-1.0Ti-0.4Zr-0.47C.

4. The 100- and 1000-hour stress-rupture life of as-cast NASA-SP was superior to commercial cast Co-base alloys up to approximately 1825° F (996° C) but inferior to the stronger Ni-base alloys over the entire temperature range tested. Stress-rupture ductility was low (1 to 3 percent) at 1500° F (816° C) but increased to about 40 percent at 2000° F (1093° C).

5. On the basis of tensile strength, the alloy was generally stronger than the commercial cast Co-base alloys above approximately 1400° F (760° C) but much weaker than the strongest Ni-base alloys over the entire temperature range tested. Average tensile elongation varied from 2 percent at 1500° F (816° C) to 30 percent at 2000° F (1093° C).

6. Despite its low Cr content, alloy NASA-SP was as resistant in high velocity cyclic oxidation tests as currently used Co-base alloys. It was lower in oxidation resistance than Ni-base alloys.

7. The thermal fatigue resistance was superior to Ni-base alloys but generally inferior to Co-base alloys.

8. Phase identification studies on as-cast NASA-SP indicated the presence of a high volume fraction of fine gamma-prime particles, large particles of a monocarbide (TiC), smaller particles of another carbide believed to be ZrC, and an unknown intermetallic rich in Al. With exposure to stress-rupture conditions the unknown intermetallic decomposed to form large islands of gamma-prime and the fine gamma-prime greatly coarsened.

Lewis Research Center,
    National Aeronautics and Space Administration,
        Cleveland, Ohio, July 14, 1969,
            129-03.

# APPENDIX A

## NOTATION FOR CONDITIONS OF INDEPENDENT VARIABLES

Let $\xi_j$, where $j = 1, \ldots, g$, be the controlled variables. Designate the serial number of each trial and observation by the subscript $i$ where $i = 1, 2, \ldots, n$. Define <u>standard levels</u> for the variables by

$$x_{ij} = \frac{\xi_{ij} - \bar{\xi}_j}{s_j} \qquad \begin{array}{l} i = 1, \ldots, n \\ j = \text{Ti, Cr, C, Al, T} \end{array} \qquad \text{(A1)}$$

For example, if $\xi_{Al}$ were percentage aluminum and two levels were investigated (e.g., 6.75 and 7.25 percent) and if pour temperature $\xi_T$ were investigated at two levels ($2850^\circ$ and $2950^\circ$ F), then

$$\bar{\xi}_{Al} = \frac{6.75 + 7.25}{2} = 7.0 \text{ percent}$$

$$\bar{\xi}_T = \frac{2850 + 2950}{2} = 2900^\circ \text{ F}$$

The means $\bar{\xi}_{Al}$ and $\bar{\xi}_T$ along with the other $\bar{\xi}_j$ variables locate the <u>design center</u> of the experiment in the original or <u>natural units</u>. The quantity $s_j$ is a <u>scale factor</u> that is adjusted so that equation (A1) will represent the upper levels with +1 and lower levels with -1. For $x_{iAl} = +1$,

$$\frac{7.25 - 7.0}{0.25} = +1$$

For $x_{iAl} = -1$,

$$\frac{6.75 - 7.0}{0.25} = -1$$

For $x_{iT} = +1$,

$$\frac{2950 - 2900}{50} = +1$$

For $x_{iT} = -1$,

$$\frac{2850 - 2900}{50} = -1$$

that is, the scale factors are $s_{Al} = 0.25$ and $s_T = 50$. (The design center is at 7.0 percent Al and $2900^O$ F for which $x_{iAl} = 0$ and $x_{iT} = 0$.)

The equivalence between the preceding notation for standardized variables and Yate's notation is given in reference 11.

# APPENDIX B

# DECISION PROCEDURES

The need for a decision procedure arises at the point of time where the question, "Is first-order model adequate?", is asked (see fig. 2). A procedure for answering this question was given in reference 7. It consists of using a·design of experiment for the first-order model that provides estimates of all the coefficients of the first-order model and also estimates of some coefficients that are viewed as sample members of higher order coefficients (usually interactions). The experimenter then forms a subjective judgment as to whether the higher order coefficients are small or large in comparison with the first-order coefficients. If he judges small then "Is first-order model adequate?" (fig. 2) is answered "Yes." An attempt to change the subjectivity of such a procedure to include a greater degree of objectivity can be made by using the procedures of references 15 and 16.

The half-normal plotting of reference 15 is as follows: The coefficient $b_o = 1.652$ of equation (3) is ignored. All other coefficients of equation (3) are ordered in the order $i = 1, 2, \ldots, n = 15$ of increasing absolute value. The sample cumulative distribution function, $F_i$ is then computed from

$$F_i = \frac{i - \frac{1}{2}}{n} \tag{B1}$$

Half-normal probability paper is constructed from the usual normal probability paper by the change of scale given in reference 15. Then the ordered coefficients are plotted as abscissas with the associated $F_i$ as ordinates as shown by figure 6. If the set of coefficients contains numbers that are essentially only error, then these numbers should fall on a straight line leading upward from the origin. Those coefficients that fall significantly to the right of such a line should be regarded as being significantly larger than error. Thus from the first-factorial experiment, $b_{Cr}$, $b_{Al}$, $b_C$, and $b_{Ti, Cr}$ (which are the coefficients of $x_{Cr}$, $x_{Al}$, $x_C$, and $x_{Ti}x_{Cr}$, respectively) might be regarded (fig. 6) as being significantly larger than error or, from a more conservative point of view, perhaps only $b_{Cr}$ would be regarded as significantly larger than error. In the case of the second factorial experiment, there are no points that clearly depart from the trend line. Other types of inferences that might be drawn from plots like figure 6 were discussed in reference 15.

A more objective analysis (known as chain pooling) is given for the results of the first-factorial experiment in reference 16. The conclusions were that $b_{Cr}$ and $b_{Al}$

(the coefficients of $x_{Cr}$ and $x_{Al}$) were clearly significant (significance point of view) and that $b_C$ and the $b_{TiCr}$ interaction (coefficients of $x_C$ and the product $x_{Ti}x_{Cr}$) were effects of less clearly established significance (screening point of view).

The results of a Yates' method calculation of the coefficient estimates of the regression equation for the second-factorial experiment are listed in table IV(c). The chain pooling procedure of reference 16 using a significance point of view resulted in the conclusion that no effect was significant. That procedure using a screening point of view suggested that the interaction between C and Al might be significant. The overall conclusion is that the first-degree model is not an adequate representation of the response surface in the vicinity of the design center of the second factorial experiment.

# APPENDIX C

# VECTOR OF STEEPEST ASCENT

Assume that a first-degree model has been fitted to two independent variables. The prediction equation is written

$$y = b_0 + b_1 x_1 + b_2 x_2 \qquad \text{(C1)}$$

Let a new observation point be $B$ at a distance $r$ from the design center, $A$. To be determined is the direction of $B$ from $A$ that will produce a maximum rate of rise. The rate of rise is the derivative of $y$ with respect to $r$:

$$\frac{\partial y}{\partial r} = \frac{\partial y}{\partial x_1} \frac{\partial x_1}{\partial r} + \frac{\partial y}{\partial x_2} \frac{\partial x_2}{\partial r} \qquad \text{(C2)}$$

Let $r$ be the length of a vector in the $x_1 - x_2$ plane. Let $\theta$ be the angle between $r$ and $x_1$. Let the increments in going from $A$ to $B$ be $\Delta r, \Delta x_1, \Delta x_2$. Then

$$\Delta x_1 = \Delta r \cos \theta \qquad \Delta x_2 = \Delta r \sin \theta$$

or equivalently

$$\frac{\partial x_1}{\partial r} = \cos \theta$$

and

$$\frac{\partial x_2}{\partial r} = \sin \theta$$

Differentiating equation (C1) gives

$$\frac{\partial y}{\partial x_1} = b_1$$

$$\frac{\partial y}{\partial x_2} = b_2$$

therefore, from equation (C2)

$$\frac{\partial y}{\partial r} = b_1 \cos \theta + b_2 \sin \theta \qquad \text{(C3)}$$

In seeking the direction of steepest ascent, the first step is to differentiate with respect to $\theta$ and then set the derivative equal to zero.

$$\frac{\partial}{\partial \theta} \frac{\partial y}{\partial r} = -b_1 \sin \theta + b_2 \cos \theta$$

$$= -b_1 \frac{\Delta x_2}{\Delta r} + b_2 \frac{\Delta x_1}{\Delta r} = 0$$

Thus

$$\frac{\Delta x_1}{b_1} = \frac{\Delta x_2}{b_2}$$

The discussion is readily generalized to any number of independent variables. The direction of steepest ascent is therefore given by

$$\frac{\Delta x_1}{b_1} = \frac{\Delta x_2}{b_2} = \frac{\Delta x_3}{b_3} = \ldots = \frac{\Delta x_g}{b_g} \qquad \text{(C4)}$$

where the signs of the $\Delta x_j$ must be the same as the signs of the $b_j$. Thus the $b_1$, $b_2$, . . ., $b_g$ might be considered to be the direction numbers of the vector of steepest ascent.

With additional significant figures, equation (4) is

$$y = 1.6522 - 0.0297 \, x_{Ti} - 0.3833 \, x_{Cr} + 0.1002 \, x_C - 0.1464 \, x_{Al} + 0.0370 \, x_T \qquad \text{(C5)}$$

and therefore equation (C4) becomes

$$\frac{\Delta x_{Ti}}{-0.0297} = \frac{\Delta x_{Cr}}{-0.3833} = \frac{\Delta x_{C}}{0.1002} = \frac{\Delta x_{Al}}{-0.1464} = \frac{\Delta x_{T}}{0.0370} \tag{C6}$$

Equation (C5) was written in design units. Equation (C6) can be converted to natural units using the scale factors listed in table II(a). The result is

$$\frac{\Delta\xi_{Ti}}{(0.5)(-0.0297)} = \frac{\Delta\xi_{Cr}}{(2.0)(-0.3833)} = \frac{\Delta\xi_{C}}{(0.1)(0.1002)} = \frac{\Delta\xi_{Al}}{(0.25)(-0.1464)} = \frac{\Delta\xi_{T}}{(50)(0.0370)} \tag{C7}$$

The decision was made to evaluate compositions along the line of steepest ascent by starting with the design center and reducing the Cr in steps of 2.0 weight percent. (Eq. (C5) suggests that Ti, Cr, and Al should be reduced and that C and pour temperature should be increased.) Thus $\Delta Cr = -2.0$ and equations (C7) give the corresponding increments in natural units of the other variables. The corresponding steps along the vector are given in table III, except that because negative values of a composition variable are impossible, the fourth point was modified from $\xi_{Cr} = -2.0$ to $\xi_{Cr} = 0.0$.

# APPENDIX D

## THE METHOD OF CANONICAL REDUCTION

The fitted prediction equation (eq. (5)) is as follows:

$$y = 2.35375 - 0.010617\ x_{Ti} + 0.013127\ x_{Cr} + 0.029996\ x_C - 0.036648\ x_{Al} - 0.085028\ x_{Ti}^2 - 0.026188\ x_{Cr}^2$$

$$- 0.026077\ x_C^2 - 0.059810\ x_{Al}^2 - 0.004357\ x_{Ti}x_{Cr} + 0.024560\ x_{Ti}x_C - 0.053884\ x_{Ti}x_{Al}$$

$$- 0.010860\ x_{Cr}x_C - 0.020984\ x_{Cr}x_{Al} + 0.077157\ x_C x_{Al} \tag{D1}$$

The next major step in the analysis is to investigate the function given by equation (D1) by the method of canonical reduction (refs. 10 and 20). Before this method can be applied, the stationary point (the point at which the tangent plane has zero slope) must be found. The first derivatives of equation (D1) are

$$\left.\begin{aligned}
\frac{\partial y}{\partial x_{Ti}} &= -0.010617 - 0.170056\ x_{Ti} - 0.004357\ x_{Cr} + 0.024560\ x_C - 0.053884\ x_{Al} \\[1em]
\frac{\partial y}{\partial x_{Cr}} &= 0.013127 - 0.052376\ x_{Cr} - 0.004357\ x_{Ti} - 0.010860\ x_C - 0.020984\ x_{Al} \\[1em]
\frac{\partial y}{\partial x_C} &= 0.029996 - 0.052154\ x_C + 0.024560\ x_{Ti} - 0.010860\ x_{Cr} + 0.077157\ x_{Al} \\[1em]
\frac{\partial y}{\partial x_{Al}} &= -0.036648 - 0.119620\ x_{Al} - 0.053884\ x_{Ti} - 0.020984\ x_{Cr} + 0.077157\ x_C
\end{aligned}\right\} \tag{D2}$$

The stationary point is to be determined by setting the derivatives in equations (D2) equal to zero. The point so determined is the point

$$x_{Ti} = 0.021503$$

$$x_{Cr} = 0.214666$$

$$x_{C} = 0.377617 \tag{D3}$$

$$x_{Al} = -0.110146$$

The point is to be converted in accordance with equations (A1) from design units to natural units in terms of the design center and scale factors of table IV(a):

$$x_{Ti} = \frac{\xi_{Ti} - 1.0}{0.5}$$

$$x_{Cr} = \frac{\xi_{Cr} - 2.0}{0.5}$$

$$x_{C} = \frac{\xi_{C} - 0.5}{0.1} \tag{D4}$$

$$x_{Al} = \frac{\xi_{Al} - 6.75}{0.25}$$

The equations that are inverses of equations (D4) are

$$\xi_{Ti} = 0.5\, x_{Ti} + 1.0$$

$$\xi_{Cr} = 0.5\, x_{Cr} + 2.0$$

$$\xi_{C} = 0.1\, x_{C} + 0.5 \tag{D5}$$

$$\xi_{Al} = 0.25\, x_{Al} + 6.75$$

The result of substituting the values given by equations (D3) into equations (D5) is

$$\xi_{Ti} = 1.01$$

$$\xi_{Cr} = 2.11$$

$$\xi_C = 0.54$$

$$\xi_{Al} = 6.72$$

The stationary point of equation (D1) is not necessarily the maximum point. The nature of the fitted response surface (eq. (D1)) is to be examined using a technique called the method of canonical reduction. The fitted function (eq. (D1)) is a quadratic surface in four variables defined in terms of coordinate axes that measure the composition variables in design units. The method of canonical reduction determines a new set of axes that are mutually perpendicular and that define the planes of symmetry of the quadratic surface. These axes have their origin at the center of symmetry of the quadratic surface, and this point is also the stationary point (which has already been determined in terms of the original axes as eqs. (D3)). Let the new axes be $v_1$, $v_2$, $v_3$, and $v_4$. Where $y_s$ is the value of the computed function at the stationary point, equation (D1) in the new coordinates is

$$y - y_s = \lambda_1 v_1^2 + \lambda_2 v_2^2 + \lambda_3 v_3^2 + \lambda_4 v_4^2 \tag{D6}$$

The values of the $\lambda$'s then give information about the function as follows:

(1) If $\lambda_1$, $\lambda_2$, . . . are all negative, the fitted surface has a true maximum at the stationary point.

(2) If one or more of the $\lambda$'s are positive, while some are negative, there is a col or minimax (saddle point) at the center of symmetry. Those values of $\lambda$ that are large and positive suggest that further experiments be performed along the associated $v$-axis.

(3) Large absolute values of $\lambda$ correspond to rapid changes of response while small values indicate a lack of sensitivity.

The fact that the values in equations (D3) are less than 1 shows that the center of symmetry is inside the range of experimentation. If the center of symmetry were computed to be outside the range of experimentation, then the second-degree model could not be trusted to represent the true response at the indicated center of symmetry. That kind of problem is discussed in pages 529 to 531 of reference 10.

Substitution of the coordinates of the stationary point (eqs. (D3)) into the prediction equation (D1) gives the value $y_s$ of the predicted response at the stationary point. Equi-

valently, an equation for the stationary point (p. 363 of ref. 8) gives

$$y_s = 2.353750 + \frac{1}{2} \Big[ (-0.010617)(0.021503)$$

$$+ (0.013127)(0.214666)$$

$$+ (0.029996)(0.377617)$$

$$+ (-0.036648)(-0.110146) \Big]$$

$$= 2.362727$$

The origin of coordinates can be shifted to the stationary point (eqs. (D3)) by the following substitutions:

$$u_{Ti} = x_{Ti} - 0.021503$$

$$u_{Cr} = x_{Cr} - 0.214666$$

$$u_C = x_C - 0.377617$$

$$u_{Al} = x_{Al} + 0.110146$$

and then

$$\left. \begin{array}{l} x_{Ti} = u_{Ti} + 0.021503 \\[2ex] x_{Cr} = u_{Cr} + 0.214666 \\[2ex] x_C = u_C + 0.377617 \\[2ex] x_{Al} = u_{Al} - 0.110146 \end{array} \right\} \qquad \text{(D7)}$$

On substituting into equation (D1),

$$y = 2.35375 - 0.010617(u_{Ti} + 0.021503) + 0.013127(u_{Cr} + 0.214666) + 0.029996(u_C + 0.377617)$$

$$- 0.036648(u_{Al} - 0.110146) - 0.085028(u_{Ti} + 0.021503)^2 - 0.026188(u_{Cr} + 0.214666)^2$$

$$- 0.026077(u_C + 0.377617)^2 - 0.059810(u_{Al} - 0.110146)^2 - 0.004357(u_{Ti} + 0.021503)(u_{Cr} + 0.214666)$$

$$+ 0.024560(u_{Ti} + 0.021503)(u_C + 0.377617) - 0.053884(u_{Ti} + 0.021503)(u_{Al} - 0.110146)$$

$$- 0.010860(u_{Cr} + 0.214666)(u_C + 0.377617) - 0.020984(u_{Cr} + 0.214666)(u_{Al} - 0.110146)$$

$$+ 0.077157(u_C + 0.377617)(u_{Al} - 0.110146)$$

If in the preceding equation $u_{Ti} = u_{Cr} = u_C = u_{Al} = 0$ then $y$ must equal its stationary point value. Therefore the constant term of the preceding equation is the value previously computed, namely, $y_s = 2.362727$. The preceding equation is therefore:

$$y = 2.362727 + [-0.010617 - 2(0.085028)(0.021503) - (0.004357)(0.214666) + (0.024560)(0.377617)$$

$$+ (0.053884)(0.110146)]u_{Ti} + [0.013127 - 2(0.026188)(0.214666) - (0.004357)(0.021503)$$

$$- (0.010860)(0.377617) + (0.020984)(0.110146)]u_{Cr} + [0.029996 - 2(0.026077)(0.377617)$$

$$+ (0.024560)(0.021503) - (0.010860)(0.214666) - (0.077157)(0.110146)]u_C + [-0.036648$$

$$+ 2(0.059810)(0.110146) - (0.053884)(0.021503) - (0.020984)(0.214666)$$

$$+ (0.077157)(0.377617)]u_{Al} - 0.085028\,u_{Ti}^2 - 0.026188\,u_{Cr}^2 - 0.026077\,u_C^2 - 0.059810\,u_{Al}^2$$

$$- 0.004357\,u_{Ti}u_{Cr} + 0.024560\,u_{Ti}u_C - 0.053884\,u_{Ti}u_{Al} - 0.010860\,u_{Cr}u_C$$

$$- 0.020984\,u_{Cr}u_{Al} + 0.077157\,u_C u_{Al}$$

Performing the indicated operations shows that the first-degree terms all vanish. The equation reduces to the form

$$y - 2.362727 = -0.085028\, u_{Ti}^2 - 0.0021785\, u_{Ti}u_{Cr} + 0.012280\, u_{Ti}u_C - 0.026942\, u_{Ti}u_{Al}$$

$$- 0.0021785\, u_{Ti}u_{Cr} - 0.026188\, u_{Cr}^2 - 0.005430\, u_{Cr}u_C - 0.010492\, u_{Cr}u_{Al}$$

$$+ 0.012280\, u_{Ti}u_C - 0.005430\, u_{Cr}u_C - 0.026077\, u_C^2 + 0.0385785\, u_C u_{Al}$$

$$- 0.026942\, u_{Ti}u_{Al} - 0.010492\, u_{Cr}u_{Al} + 0.0385785\, u_C u_{Al} - 0.059810\, u_{Al}^2 \tag{D8}$$

The preceding equation is known as a homogeneous quadratic form. The coefficients can be written as a symmetric matrix using the array as shown. As developed in reference 20, characteristic roots, $\lambda_i$ of the coefficient matrix together with associated characteristic vectors can be computed. The array of normalized characteristic vectors is called the modal matrix, M.

The matrix representation of equation (D8) is

$$y - 2.362727 = U^T A U = [u_{Ti}u_{Cr}u_C u_{Al}] \begin{bmatrix} -0.085028 & -0.0021785 & 0.012280 & -0.026942 \\ -0.0021785 & -0.026188 & -0.005430 & -0.010492 \\ 0.012280 & -0.005430 & -0.026077 & 0.0385785 \\ -0.026942 & -0.010492 & 0.0385785 & -0.059810 \end{bmatrix} \begin{bmatrix} u_{Ti} \\ u_{Cr} \\ u_C \\ u_{Al} \end{bmatrix}$$

where A is the array of coefficients of equation (D8).

The characteristic roots of A as determined by a machine computation are

$$\lambda_1 = -0.114796 \qquad \lambda_2 = -0.029290 \qquad \lambda_3 = 0.003072 \qquad \lambda_4 = -0.056089$$

The canonical form of equations (D1) or (D8) was given as equation (D6) which can now be written as

$$y - 2.362727 = -0.114796\, v_1^2 - 0.029290\, v_2^2 + 0.003072\, v_3^2 - 0.056089\, v_4^2 \tag{D9}$$

Equation (D9) shows that y decreases for any point that moves away from the origin (stationary point) along the $v_1$, $v_2$, or $v_4$ axes. The equation also suggests that y might increase slowly if a point is moved in either direction from the origin along the $v_3$ axis.

The modal matrix from a machine computation is

$$
M = \begin{bmatrix}
0.704176 & 0.067499 & -0.358275 & 0.609277 \\
-0.017058 & 0.937416 & 0.329975 & 0.109899 \\
-0.052589 & -0.334483 & 0.765082 & 0.547728 \\
-0.707869 & 0.069407 & -0.421196 & 0.562759
\end{bmatrix}
$$

The coefficients of the transformation from $U$ to $V$ are in the rows of $M$; that is, $V = MU$. Using the transformation from $U$ to $X$ in terms of the stationary point the transformation from $X$ to $V$ is

$$v_1 = 0.704176(x_{Ti} - 0.021503) + 0.067499(x_{Cr} - 0.214666) - 0.358275(x_C - 0.377617) + 0.609277(x_{Al} + 0.110146)$$

$$v_2 = -0.017058(x_{Ti} - 0.021503) + 0.937416(x_{Cr} - 0.214666) + 0.329975(x_C - 0.377617) + 0.109899(x_{Al} + 0.110146)$$

$$v_3 = -0.052589(x_{Ti} - 0.021503) - 0.334483(x_{Cr} - 0.214666) + 0.765082(x_C - 0.377617) + 0.547728(x_{Al} + 0.110146)$$

$$v_4 = -0.707869(x_{Ti} - 0.021503) + 0.069407(x_{Cr} - 0.214666) - 0.421196(x_C - 0.377617) + 0.562759(x_{Al} + 0.110146)$$

Using the transformation $V = MU$ a series of compositions can be determined along the $v_3$ axis that should have as good or better properties than the composition at the stationary point. Equation (D9) suggests that the stress-rupture life decreases along the $v_1$, $v_2$, and $v_4$ axes and that it increases very slowly along the $v_3$ axis. These observations suggest that a particularly interesting sequence of compositions may be determined by setting $v_1 = v_2 = v_4 = 0$ and allowing $v_3$ to take on a sequence of values of increasing absolute magnitude. But to retain the validity of the model, the sequence of compositions should be kept essentially within the experimental space that has already been explored. Suitable values might be $v_3 = 0$, $\pm0.5$, $\pm1.0$, $\pm1.5$, and $\pm2.0$.

Because  M  is an orthonormal matrix, the transformation from  V  to  U  is easily determined:

$$V = MU$$

$$M^{-1}V = U$$

$$U = M^T V$$

where  $M^T$  is the transpose of  M.  Thus

$$u_{Ti} = 0.704176\, v_1 - 0.017058\, v_2 - 0.052589\, v_3 - 0.707869\, v_4$$

$$u_{Cr} = 0.067499\, v_1 + 0.937416\, v_2 - 0.334483\, v_3 + 0.069407\, v_4$$

$$u_{C} = -0.358275\, v_1 + 0.329975\, v_2 + 0.765082\, v_3 - 0.421196\, v_4$$

$$u_{Al} = 0.609277\, v_1 + 0.109899\, v_2 + 0.547728\, v_3 + 0.562759\, v_4$$

Setting  $v_1 = v_2 = v_4 = 0$  yields

$$u_{Ti} = -0.052589\, v_3$$

$$u_{Cr} = -0.334483\, v_3$$

$$u_{C} = 0.765082\, v_3$$

$$u_{Al} = 0.547728\, v_3$$

Using the transformation from  X  to  U  in terms of the stationary point (eq. (D7)) yields

$$\left.\begin{aligned}
x_{Ti} &= 0.021503 - 0.052589\, v_3 \\[6pt]
x_{Cr} &= 0.214666 - 0.334483\, v_3 \\[6pt]
x_{C} &= 0.377617 + 0.765082\, v_3 \\[6pt]
x_{Al} &= -0.110146 + 0.547728\, v_3
\end{aligned}\right\} \qquad \text{(D10)}$$

Using the transformation from design units to compositions in weight percents (eqs. (D5)) results in

$$\xi_{Ti} = 1.0 + 0.5(0.021503 - 0.052589\ v_3)$$

$$\xi_{Cr} = 2.0 + 0.5(0.214666 - 0.334483\ v_3)$$

$$\xi_C = 0.5 + 0.1(0.377617 + 0.765082\ v_3)$$

$$\xi_{Al} = 6.75 + 0.25(-0.110146 + 0.547728\ v_3)$$

from which

$$\left.\begin{aligned}
\xi_{Ti} &= 1.010752 - 0.026295\ v_3 \\[4pt]
\xi_{Cr} &= 2.107333 - 0.167242\ v_3 \\[4pt]
\xi_C &= 0.537762 + 0.076508\ v_3 \\[4pt]
\xi_{Al} &= 6.722463 + 0.136932\ v_3
\end{aligned}\right\} \tag{D11}$$

# APPENDIX E

# ELONGATION AS A SECOND DEPENDENT VARIABLE

In order to consider a second dependent variable, an equation having a form given by equation (1) was fitted to the elongation data of tables IV(b) and V. This equation was solved for the previously listed values of $v_3$ through the relations (eqs. (D10) between $v_3$ and $x_{Ti}$, $x_{Cr}$, $x_C$, and $x_{Al}$ (which had been determined in terms of stress-rupture data). The solution is shown by figure 20. The graph shows that improved elongation should be expected with increasing values of $v_3$. The composition variables associated with these values of $v_3$ were computed using equations (D11) and are shown by table X. The range of the experimenting is essentially defined by table IV(a). Comparison of table X with table IV(a) shows that all the values of $v_3$ of table X led to compositions within
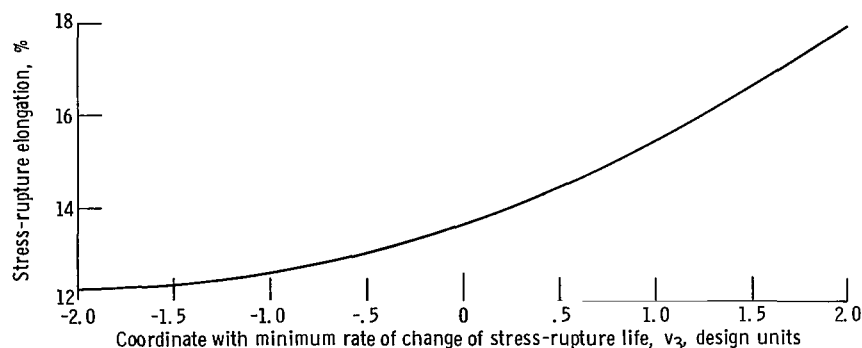


Figure 20. – Elongation values along rising ridge of stress-rupture response surface model. (Compositions in natural units given as function of $v_3$ in table X.) Temperature, 1850° F (1010° C); stress, 15 ksi (103 MN/m$^2$).

TABLE X. – LEVELS OF ELEMENTS ALONG

SLOWLY RISING RIDGE OBTAINED

FROM EQUATIONS (D11)

| $v_3$ | Level, wt. % | | | |
|---|---|---|---|---|
| | $\xi_{Ti}$ | $\xi_{Cr}$ | $\xi_C$ | $\xi_{Al}$ |
| -2.0 | 1.063342 | 2.441817 | 0.384746 | 6.448599 |
| -1.5 | 1.050194 | 2.358196 | .423000 | 6.517065 |
| -1.0 | 1.037047 | 2.274575 | .461254 | 6.585531 |
| -.5 | 1.023900 | 2.190954 | .499508 | 6.653997 |
| .0 | 1.010752 | 2.107333 | .537762 | 6.722463 |
| .5 | .997604 | 2.023712 | .576016 | 6.790929 |
| 1.0 | .984457 | 1.940091 | .614270 | 6.859395 |
| 1.5 | .971310 | 1.856470 | .652524 | 6.927861 |
| 2.0 | .958162 | 1.772849 | .690778 | 6.996327 |

the ranges of table IV(a) except that the smallest value of $v_3$ and the two largest values of $v_3$ gave values of $\xi_C$ that were clearly outside the ranges of table IV(a). In summary, a value of $v_3 = 1$ constitutes a negligible extrapolation of the data fit and figure 20 suggests that the associated elongation would be 15.5 percent as compared with 13.7 percent for the stationary point ($v_3 = 0$).

In conclusion, if additional experimenting were to be done, it would reasonably consist of melting and testing the compositions listed in table X for two reasons:

(1) The canonical reduction of the equation fitted to the time to rupture data had suggested that with $v_1 = v_2 = v_4 = 0$ small improvements in stress-rupture life might occur with positive or negative values of $v_3$.

(2) With $v_1 = v_2 = v_4 = 0$, the changes in stress-rupture life with $v_3$ are very small, but figure 20 suggests that improvements in ductility are to be expected with increases in $v_3$. Thus experiments corresponding to $v_1 = v_2 = v_4 = 0$ with increasing $v_3$ might show useful increases in ductility with negligible decreases, or possibly small increases, in stress-rupture life.

# APPENDIX F

## ANALYSIS OF VARIANCE WITH UNEQUAL SUBCLASSES

## TO INVESTIGATE MELT VARIABILITY

## AND COMPOSITION CHANGES

The purpose of the analysis in this appendix is to answer two questions:

(1) Is the melt-to-melt variability of rupture life significantly larger than the variability of rupture lives of test bars from a single melt?

(2) Is the difference between rupture life for the design center composition of the second-factorial experiment and the rupture life for the stationary point composition significantly larger than the melt-to-melt variability?

In addition, some estimates will be given for the components of the total standard deviation.

The analysis to answer these questions could be performed directly in terms of the observed rupture times or in terms of the logarithmic transformation of the rupture times. The Box-Wilson model fitting was done in terms of log times so that the error variance would be approximately constant over large variations (as much as 68 to 1 in table II(b)). On the other hand, the data for the present analysis (the four melts of table V with center-point compositions and the two melts of table VI(b)) show a maximum variation of only 1.5 to 1. The logarithmic transformation was not used and the analysis therefore provided estimates of components of the total standard deviation directly in terms of hours.

The available data consist of the four melts of table V (alloys C-1 to C-4) and the two melts of table VI(b) (alloys SP-1 and SP-2). The effects to be investigated are the fixed effect of the change in composition and the random effect of the melts. The melt effects are nested within the composition effects. In the present set of data the replication error variance (the bar-to-bar variability) is to be estimated from the equal numbers of bars (two) within each melt. The class effects of melts is to be estimated from the unequal numbers of melts (four and two) within the composition classes.

The case of unequal numbers of subclasses is treated by Graybill in pages 354-359 of reference 21. In that reference, the main classes are assumed to have randomly distributed means, whereas, in the present investigation, the two compositions are assumed to be fixed effects. The model representing the total situation is thus a mixed model consisting of the fixed main classes (compositions) and the random subclasses (melts). The formulation of the model uses notation similar to that used by Bennett and Franklin for nested classifications in pages 358-368 of reference 22. The model is as follows:

$$i = 1, 2, \ldots, l \qquad l = 2 \text{ compositions}$$

$$j = 1, 2, \ldots, m_i \qquad m_i = 2, 4 \text{ melts within compositions}$$

$$k = 1, 2, \ldots, n \qquad n = 2 \text{ bars within each melt}$$

Where $t_{ijk}$ is the observed rupture time, the assumed analysis of variance model will be

$$t_{ijk} = \mu_i + z_{j(i)} + \epsilon_{k(ij)} \tag{F1}$$

In the preceding equation $\epsilon_{k(ij)}$ is defined to be the error due to testing and to variation within melts and it is assumed to be independently, normally distributed with mean zero and constant variance $\sigma^2_{k(ij)}$. The quantity $\mu_i$ is assumed to be the population mean for any one composition, and the mean value within any one melt is assumed to differ from $\mu_i$ by an amount $z_{j(i)}$ where $z_{j(i)}$ is assumed to be independently normally distributed with population mean zero and constant variance $\sigma^2_{j(i)}$.

Functions of the observations are defined as follows:

$$T_{j(i)} = \sum_{k=1}^{n} t_{ijk}$$

$$\overline{t}_{j(i)} = \frac{1}{n} T_{j(i)}$$

$$T_i = \sum_{j=1}^{m_i} T_{j(i)}$$

$$\overline{t}_i = \frac{1}{nm_i} T_i$$

$$T = \sum_{i=1}^{l} T_i$$

$$N = \sum_{i=1}^{\ell} nm_i$$

$$\overline{t} = \frac{1}{N} T$$

$$C_{(ijk)} = \sum_{i=1}^{\ell} \sum_{j=1}^{m_i} \sum_{k=1}^{n} t_{ijk}^2$$

$$C_{(ij)} = \sum_{i=1}^{\ell} \sum_{j=1}^{m_i} \frac{T_{j(i)}^2}{n}$$

$$C_{(i)} = \sum_{i=1}^{\ell} \frac{T_i^2}{nm_i}$$

$$C = \frac{T^2}{N}$$

$$S_i = C_{(i)} - C$$

$$S_{j(i)} = C_{(ij)} - C_{(i)}$$

$$S_{k(ij)} = C_{(ijk)} - C_{(ij)}$$

$$S = C_{(ijk)} - C$$

A partitioning of the sums of squares shows that

$$S = S_i + S_{j(i)} + S_{k(ij)} \tag{F2}$$

where $S_i$ represents the variation of composition means with respect to the grand mean,

$S_{j(i)}$ represents the variation of melt means within a given composition with respect to the composition mean, and $S_{k(ij)}$ represents the variation of individual bars within any given melt.

The detailed computations of sums of squares are as follows:

| | | k = 1 | k = 2 | $T_{j(i)}$ | $T_i$ | T |
|---|---|---|---|---|---|---|
| i = 1 | j = 1 | 279.3 | 269.7 | 549.0 | | |
| | j = 2 | 198.4 | 172.1 | 370.5 | | |
| | j = 3 | 233.6 | 203.9 | 437.5 | | |
| | j = 4 | 242.8 | 227.3 | 470.1 | | |
| $m_1 = 4$ | | 954.1 | 873.0 | | 1827.1 | |
| i = 2 | j = 1 | 186.0 | 203.3 | 389.3 | | |
| | j = 2 | 203.7 | 196.2 | 399.9 | | |
| $m_2 = 2$ | | 389.7 | 399.5 | | 789.2 | |
| | | | | | | 2616.3 |

$$C_{(ijk)} = \sum_{i=1}^{l} \sum_{j=1}^{m_i} \sum_{k=1}^{n} t_{ijk}^2 = 582\ 403.870$$

$$C_{(ij)} = \sum_{i=1}^{l} \sum_{j=1}^{m_i} \frac{T_{j(i)}^2}{n} = \frac{1\ 162\ 546.01}{2} = 581\ 273.005$$

$$C_{(i)} = \sum_{i=1}^{l} \frac{T_i^2}{nm_i} = \frac{3\ 338\ 294.41}{8} + \frac{622\ 836.64}{4}$$

$$= 417\ 286.801 + 155\ 709.160 = 572\ 995.961$$

$$C = \frac{T^2}{N} = \frac{6\ 845\ 025.69}{12} = 570\ 418.808$$

$$S_i = C_{(i)} - C = 2577.153$$

$$S_{j(i)} = C_{(ij)} - C_{(i)} = 8277.044$$

$$S_{k(ij)} = C_{(ijk)} - C_{(ij)} = 1130.865$$

$$S = C_{(ijk)} - C = 11\ 985.062$$

Where a mean square is defined as a sum of squares divided by the associated degrees of freedom, the analysis of variance table that is consistent with the model equation (F1) and that has expected mean squares given by Graybill (ref. 21), is

| Sum of squares | Degrees of freedom | Mean square | Expectation of mean square |
|---|---|---|---|
| $S_i$ | $l - 1$ | $MS_i$ | $\sigma^2_{k(ij)} + q_1\sigma^2_{j(i)} + q_2\sigma^2_i$ |
| $S_{j(i)}$ | $\displaystyle\sum_{i=1}^{l}(m_i - 1)$ | $MS_{j(i)}$ | $\sigma^2_{k(ij)} + q_0\sigma^2_{j(i)}$ |
| $S_{k(ij)}$ | $\displaystyle\sum_{i=1}^{l} m_i(n - 1)$ | $MS_{k(ij)}$ | $\sigma^2_{k(ij)}$ |
| $S$ | $\displaystyle\sum_{i=1}^{l}(nm_i) - 1$ | | |

In the preceding table, $\sigma^2_i$ is not the variance of a random variable but is merely a function of the fixed parameters $\mu_i$.

$$q_0 = \frac{N - \dfrac{\displaystyle\sum_{i=1}^{l}\dfrac{\displaystyle\sum_{j=1}^{m_i}n^2}{nm_i}}{1}}{\displaystyle\sum_{i=1}^{l}(m_i - 1)}$$

$$q_1 = \frac{\sum_{i=1}^{l}\sum_{j=1}^{m_i}\left(\frac{n^2}{nm_i} - \frac{n^2}{N}\right)}{l - 1}$$

$$q_2 = \frac{N - \dfrac{\sum_{i=1}^{l}(nm_i)^2}{N}}{l - 1}$$

For the given experiment and in the preceding equations, $n = 2$, $m_1 = 4$, $m_2 = 2$, $l = 2$, $N = 12$.

$$q_0 = \frac{12 - \left[\dfrac{4(2)^2}{2(4)} + \dfrac{2(2)^2}{2(2)}\right]}{(4 - 1) + (2 - 1)} = 2$$

$$q_1 = \frac{4\left[\dfrac{2^2}{2(4)} - \dfrac{2^2}{12}\right] + 2\left[\dfrac{2^2}{2(2)} - \dfrac{2^2}{12}\right]}{2 - 1} = 2$$

$$q_2 = \frac{12 - \dfrac{1}{12}\left\{\left[2(4)\right]^2 + \left[2(2)\right]^2\right\}}{2 - 1} = \frac{16}{3}$$

Under the null hypothesis that $\sigma^2_{j(i)} = 0$, the ratio $MS_{j(i)}/MS_{k(ij)}$ has the F-distribution with $\sum_{i=1}^{l}(m_i - 1)$ and $\sum_{i=1}^{l} m_i(n - 1)$ degrees of freedom.

Under the null hypothesis that $\mu_1 = \ldots = \mu_l$ the test of such a hypothesis recognizes that "melts" is a classification nested within "compositions," and therefore the appropriate test statistic is $MS_i/MS_{j(i)}$. Because in the present situation $q_1 = q_0$, under the null hypothesis $MS_i/MS_{j(i)}$ has the F-distribution with $l - 1$ and $\sum_{i=1}^{l}(m_i - 1)$ degrees of freedom.

The analysis of variance computations are as follows:

| Source | Sum of squares | Degrees of freedom | Mean square | F-ratio |
|---|---|---|---|---|
| Compositions | 2577. 153 | 1 | 2577. 153 | 1. 245 |
| Melts | 8277. 044 | (4 - 1) + (2 - 1) = 4 | 2069. 261 | 10. 979 |
| Bars | 1130. 865 | 6(2 - 1) = 6 | 188. 478 | ------ |

The conclusions of the analysis of variance are as follows:

(1) Considering the null hypothesis that $\sigma^2_{j(i)} = 0$, the computed F-ratio was 10.979, which is to be compared at a significance level of $\alpha = 0.01$ with a critical F-ratio for 4 and 6 degrees of freedom of 9.1483. The melt-to-melt variation is significantly larger than the bar-to-bar variation.

(2) Considering the null hypothesis that $\mu_1 = \mu_2$, the computed F-ratio was 1.245, but at a significance level of $\alpha = 0.25$ the critical F-ratio for 1 and 4 degrees of freedom is 1.8074. The difference in mean rupture lives of the two compositions is not at all significant in comparison with the melt-to-melt variation.

The estimates of the sample standard deviation due to stress-rupture testing and variability within melts (i. e., the bar-to-bar variation $\hat{\sigma}_{k(ij)}$ and the standard deviation due to melt variability $\hat{\sigma}_{j(i)}$) and the overall variability for any given composition (i. e., the standard deviation associated with melting one melt and testing one bar from it $\hat{\sigma}$) are obtained as follows:

$$\hat{\sigma}^2_{k(ij)} + n\hat{\sigma}^2_{j(i)} = \hat{\sigma}^2_{k(ij)} + 2\hat{\sigma}^2_{j(i)} = 2\,069.261$$

$$\hat{\sigma}^2_{k(ij)} = 188.478$$

$$2\hat{\sigma}^2_{j(i)} = 1\,880.783$$

$$\hat{\sigma}^2_{j(i)} = 940.392$$

$$\hat{\sigma}_{k(ij)} = (188.478)^{1/2} = 13.7 \text{ hr}$$

$$\hat{\sigma}_{j(i)} = (940.392)^{1/2} = 30.7 \text{ hr}$$

$$\hat{\sigma} = (188.478 + 940.392)^{1/2} = 33.6 \text{ hr}$$

The estimates of variances are unbaised estimates, and some of them (depending on sampling variability) could be negative quantities. Alternative estimation theories have

been proposed for such cases. For negative estimates, the conclusion that is consistent with the elementary usage of the unbiased estimation theory is that the corresponding population parameter is zero.

# REFERENCES

1. Guard, R. W.; and Prater, T. A.: An Austenitic Alloy for High Temperature Use. Trans. ASM, vol. 49, 1957, pp. 842-861.

2. Rogister, C.; Coutsouradis, D.; and Habraken, L.: Improvement of Heat-Resisting Cobalt-Base Alloys by Precipitation Hardening. Cobalt, no. 34, Mar. 1967, pp. 3-9.

3. Bollenrath, F.; and Rohde, W.: Precipitation-Hardening Behaviour and Mechanical Properties of Heat-Resisting Alloys Containing up to 35 Percent Cobalt. Cobalt, no. 34, Mar. 1967, pp. 18-36.

4. Collins, H. E.; Quigg, R. J.; and Dreshfield, R. L.: Development of a Nickel-Base Superalloy Using Statistically Designed Experiments. Trans. ASM, vol. 61, no. 4, Dec. 1968, pp. 711-721.

5. Brickner, K. G.; and Geissler, J. J.: The Application of Computers and Statistically Designed Experiments to Obtain Models Used in Alloy Development. Paper TR-P14-2-64, presented at the ASM Metals/Materials Congress, Philadelphia, Oct. 19-23, 1964.

6. Freche, J. C.; Ashbrook, R. L.; and Sandrock, G. D.: High-Temperature, Cobalt-Tungsten Alloys for Aerospace Applications. J. Eng. Ind., vol. 87, no. 1, Feb. 1965, pp. 9-20.

7. Box, G. E. P.; and Wilson, K. B.: On the Experimental Attainment of Optimum Conditions. J. Roy. Stat. Soc., Ser. B, vol. 13, 1951, pp. 1-45.

8. Cochran, William G.; and Cox, Gertrude M.: Experimental Designs. Second ed., John Wiley & Sons, Inc., 1957, pp. 367-368.

9. Hill, William J.; and Hunter, William G.: A Review of Response Surface Methodology. A Literature Survey. Technometrics, vol. 8, no. 4, Nov. 1966, pp. 571-590.

10. Davies, Owen L., ed.: The Design and Analysis of Industrial Experiments. Second ed., Hafner Publishing Co., 1960.

11. Holms, Arthur G.: Designs of Experiments as Telescoping Sequences of Blocks for Optimum Seeking (as Intended for Alloy Development). NASA TN D-4100, 1967.

12. Johnston, J. R.; and Ashbrook, R. L.: Oxidation and Thermal Fatigue Cracking of Nickel and Cobalt Base Alloys in a High Velocity Gas Stream. NASA TN D-5376, 1969.

13. Kriege, Owen H.; and Sullivan, C. P.: The Separation of Gamma Prime from Udimet 700. Trans, ASM, vol. 61, no. 2, June 1968, pp. 278-282.

14. Sims, Chester T.: A Contemporary View of Nickel-Base Superalloys. J. Metals, vol. 18, no. 10, Oct. 1966, pp. 1119-1130.

15. Daniel, Cuthbert: Use of Half-Normal Plots in Interpreting Factorial Two-Level Experiments. Technometrics, vol. 1, no. 4, Nov. 1959, pp. 311-341.

16. Holms, Arthur G.; and Berrettoni, J. N.: Multiple Decision Procedures for ANOVA of Two-Level Factorial Fixed-Effects Replication-Free Experiments. NASA TN D-4272, 1967.

17. Box. G. E. P.; and Hunter, J. S.: Multi-Factor Experimental Designs for Exploring Response Surfaces. Ann. Math. Stat., vol. 28, 1957, pp. 195-241.

18. Simmons, Ward F.: Rupture Strengths of Selected High-Iron, Nickel-Base, Cobalt-Base, and Refractory Metal Alloys. DMIC Memo 236, Battelle Memorial Inst., May 1, 1968. (Available from DDC as AD-670-153.)

19. Anon.: High Temperature High Strength Nickel Base Alloys. International Nickel Co., 1964.

20. Stoll, Robert R.: Linear Algebra and Matrix Theory. McGraw-Hill Book Co., Inc., 1952.

21. Graybill, Franklin A.: An Introduction to Linear Statistical Models. Vol. I. McGraw-Hill Book Co., Inc., 1961.

22. Bennett, Carl A.; and Franklin, Norman L.: Statistical Analysis in Chemistry and the Chemical Industry. John Wiley & Sons, Inc., 1954.

**FIRST CLASS MAIL**
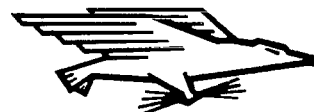
POSTAGE AND FEES PAID
NATIONAL AERONAUTICS AND
SPACE ADMINISTRATION

C3U 001 42    5L 30S           69328    00903
AIR FCRCE WEAPCNS LABCRATORY/WLIL/
KIRTLAND AIR FURCE PASE, NEW MEXICC 8711

AII E. LCU PCWMAN, CHIEF,TECH. LIPRARY

POSTMASTER:  If Undeliverable (Section 158 Postal Manual) Do Not Return

"*The aeronautical and space activities of the United States shall be conducted so as to contribute . . . to the expansion of human knowledge of phenomena in the atmosphere and space. The Administration shall provide for the widest practicable and appropriate dissemination of information concerning its activities and the results thereof.*"

— NATIONAL AERONAUTICS AND SPACE ACT OF 1958

# NASA SCIENTIFIC AND TECHNICAL PUBLICATIONS

**TECHNICAL REPORTS:** Scientific and technical information considered important, complete, and a lasting contribution to existing knowledge.

**TECHNICAL NOTES:** Information less broad in scope but nevertheless of importance as a contribution to existing knowledge.

**TECHNICAL MEMORANDUMS:** Information receiving limited distribution because of preliminary data, security classification, or other reasons.

**CONTRACTOR REPORTS:** Scientific and technical information generated under a NASA contract or grant and considered an important contribution to existing knowledge.

**TECHNICAL TRANSLATIONS:** Information published in a foreign language considered to merit NASA distribution in English.

**SPECIAL PUBLICATIONS:** Information derived from or of value to NASA activities. Publications include conference proceedings, monographs, data compilations, handbooks, sourcebooks, and special bibliographies.

**TECHNOLOGY UTILIZATION PUBLICATIONS:** Information on technology used by NASA that may be of particular interest in commercial and other non-aerospace applications. Publications include Tech Briefs, Technology Utilization Reports and Notes, and Technology Surveys.

*Details on the availability of these publications may be obtained from:*

**SCIENTIFIC AND TECHNICAL INFORMATION DIVISION**

**NATIONAL AERONAUTICS AND SPACE ADMINISTRATION**
**Washington, D.C. 20546**